DOKUZ EYLÜL UNIVERSITY
GRADUATE SCHOOL OF NATURAL AND APPLIED SCIENCES

COMPUTER AIDED ANALYSIS AND EXPERIMENTAL INVESTIGATIONS TOWARDS OPTIMIZING THE DESIGN PARAMETERS OF DOMESTIC REFRIGERATORS

by
Hasan AVCI

June, 2011
İZMİR

COMPUTER AIDED ANALYSIS AND EXPERIMENTAL INVESTIGATIONS TOWARDS OPTIMIZING THE DESIGN PARAMETERS OF DOMESTIC REFRIGERATORS

A Thesis Submitted to the

Graduate School of Natural and Applied Sciences of

Dokuz Eylül University

In Partial Fulfillment of the Requirements for the Degree of Master of Science in Mechanical Engineering, Energy Program

by

Hasan AVCI

June, 2011

İZMİR

M.Sc THESIS EXAMINATION RESULT FORM

We have read the thesis entitled **"COMPUTER AIDED ANALYSIS AND EXPERIMENTAL INVESTIGATIONS TOWARDS OPTIMIZING THE DESIGN PARAMETERS OF DOMESTIC REFRIGERATORS"** completed by **HASAN AVCI** under supervision of **ASSOC. PROF. DR. DİLEK KUMLUTAŞ** and we certify that in our opinion it is fully adequate, in scope and in quality, as a thesis for the degree of Master of Science.

Assoc. Prof. Dr. Dilek KUMLUTAŞ
Supervisor

Prof. Dr. İsmail H. TAVMAN
(Jury Member)

Asst. Prof. Dr. M. Turhan ÇOBAN
(Jury Member)

Prof. Dr. Mustafa SABUNCU
Director
Graduate School of Natural and Applied Sciences

ACKNOWLEDGEMENTS

First of all, I would like to thank my supervisor, Assoc. Prof. Dr. Dilek KUMLUTAŞ, for her incomparable knowledge and moral support, valuable advises and guidance throughout this thesis study.

This study is supported by the Ministry of Industry and Commerce, with the 00457.STZ.2009-2 encoded SANTEZ project and Vestel White Goods Company. I would like to express my gratitude about being in this project.

I also wish to express my gratitude to Assist. Ziya Haktan KARADENİZ and my friends at Department of Mechanical Engineering Energy program for their patience and help.

Finally, I would like to gratefully thanks to my family for their endless encouragement, patience and valuable support in every part of my life.

Hasan AVCI

COMPUTER AIDED ANALYSIS AND EXPERIMENTAL INVESTIGATIONS TOWARDS OPTIMIZING DESIGN PARAMETERS OF DOMESTIC REFRIGERATORS

ABSTRACT

The aim of this study is to determine the inner design parameters of the domestic refrigerators which are used to store for long time without deterioration of the quality of food product and investigate the optimum values of these parameters. Thus, the interior air volume of a single door static type refrigerator was modeled using the Computational Fluid Dynamics and Heat Transfer (CFDHT) method and analyses were made. The numerical results were validated by comparing with the experimental results from the producer company test rooms and then the inner design parameters were determined by using the numerical thermal and velocity distribution results. The optimization study of these obtained design parameter's values was made by using the both of the parametric and Artificial Neural Networks (ANNs) methods. So, it was possible to predict the optimum values of design parameter without the trial and error method which is expensive and take long time. The success of this study is to develop an optimization method for domestic refrigerators in the design and improvement process.

Keywords: Domestic refrigerators, computational fluids dynamics and heat transfer, artificial neural networks.

EV TİPİ BUZDOLAPLARININ TASARIM PARAMETERELERİNİN OPTİMİZE EDİLMESİNDE DENEYSEL ARAŞTIRMALAR VE BİLGİSAYAR DESTEKLİ ANALİZ

ÖZ

Bu çalışmanın amacı, evlerde kullanılan ve gıdaları besin değerlerini kaybetmeden uzun sure saklayabilen buzdolaplarına ait iç tasarım parametrelerinin belirlenmesi ve en uygun değerlerinin araştırılmasıdır. Bu amaçla tek kapılı statik tip bir buzdolabı iç hava hacmi, Hesaplamalı Akışkanlar Dinamiği ve Isı Transferi (HADIT) yöntemi kullanılarak modellenmiş ve analizler gerçekleştirilmiştir. Modelin doğruluğu test odasında yapılan deney sonuçlarıyla karşılaştırılarak ispatlandıktan sonra sayısal sonuçlardan elde edilen sıcaklık ve hız dağılımları incelenerek iç tasarım parametreleri belirlenmiştir. Elde edilen parametre değerlerine ait optimizasyon çalışması, parametrik ve Yapay Sinir Ağları (YSA) yöntemleri kullanılarak gerçekleştirilmiştir. Böylece, pahalı ve uzun zaman alan deneme yanılma yöntemi kullanılmaksızın tasarım parametrelerinin en iyi değerlerinin tahmin edilmesi mümkün kılınmıştır. Bu çalışmanın başarısı, tasarım ve iyileştirme aşamasında ev tipi buzdolapları için optimizasyon yöntemi geliştirmiş olmaktır.

Anahtar sözcükler: Ev tipi buzdolapları, hesaplamalı akışkanlar dinamiği ve ısı transferi, yapay sinir ağları.

CONTENTS

Page

CHAPTER ONE
LITERATURE SURVEY

1.1 Literature

The aim of this study is to optimize the design parameters of the domestic refrigerator that is determined by the experimental and the numerical investigations, with using the parametric study and the artificial neural networks (ANNs) method. A desired storage condition for food products inside the refrigerators depends on the temperature distribution of the interior volume. In addition, the intended temperatures values are provided by refrigeration system design; the proper temperature distribution is attained with the inner design. Therefore, the inner design appropriateness of the refrigerators should be investigated by observing the temperature and the flow fields of the internal volume.

It is seen from the literature that the numerical methods could be used with an acceptable level of confidence for studying the heat transfer and the fluid flow inside the refrigerators. In order to attain the best internal design for a domestic freezer, modeled 3D interior air volume for eighteen different designs were analyzed to use the Computational Fluid Dynamics (CFD) method and were verified with experimental values in the study of Saedodin, Torabi, Naserion, & Salehi (2010).

In the studies of Laguerre, & Flick, (2004) and Amara, Laguerre, Mojtabi, Lartigue, & Flick (2008), the effects of temperature and the surface area of the evaporator were studied. In that study it was found that temperature stratification in the vertical direction was observed with the cold zone at the bottom and warm zone at the top of the refrigerator cavity and distribution of these zones changed with the location and temperature of evaporator surface. So, this study gives ideas about the effect of evaporator size and temperature for selecting a design parameter as like in our study.

With the using numerical studies, in the literature were noted that could be done on the investigations of identifying problem areas and/or improvement of the design. In order to minimize that the heat transfer of domestic refrigerator through the condenser and compressor surfaces by radiation, determination the location of radiation shield on the refrigerator's external surfaces, a sheet of aluminum foil, were examined both numerically and experimentally in the study of Afonso & Matos (2006). It was found that result from experimental apparatus and from simulations shows that there is a good agreement between them which validates the experiments carried out. According to this study, the modifications of refrigerators' design were observed to find out that its effect on overall heat transfer by using CFD methods.

Another similar design study was made to investigate the problematic sections of commercial type refrigerator by Foster, Madge, & Evans (2005). In this study, these problematic sections were improved by numerical analysis and implementing the improvements on a refrigerator reduced the average power consumption from 1.37 to 1.29 kW. Traditional method of trial and error was used instead of the methodology of CFD that would be taken a long time to fix a problematic section.

A few studies were made to determine the critical design values by researchers such as Cortella, Manzan, & Comini (2001), D'agaro, Cortella, & Croce (2006), and Gupta, Gopal, Ram, & Chakraborty (2007). Modified designs were tried to obtain a more uniform temperature distribution inside the refrigerators' internal volume by Ding, Qiao, & Lu (2004). They analyzed the 2D model static type of refrigerator and shown that, the gaps between the shelves and the back wall and between the door shelves and the door are important design parameters. So, based on this investigation, these gaps taken into account in our study.

Another important study was made by Fukuyo, Taichi, & Haruko (2003) which was created the new design of air supply system to reduce undesirable high temperature at the top region of the fresh food compartment inside the refrigerator. Both of them were executed numerical method and then were verified with experimental results.

In the literature, after the verification of created numerical refrigerators' models is done by experimental studies, there isn't detailed study for optimizing the determined internal design parameters. Many engineering applications depend on the correlations of between input and output parameters. These relations of independent variables are complex and non-linear problems. ANNs is one of the optimization methods that can perform predictions and generalizations at high speed. They have been used in diverse applications such as control, robotics, pattern processing, forecasting, signal processing, manufacturing and optimization of energy systems.

A review study was made by Kalogirou (2000) that was compiled the applications of artificial neural networks for energy systems in the literature. This study which included the use of ANNs in heating, ventilating and air conditioning systems, solar radiation, power generation and refrigeration system showed the capability of ANNs as method in prediction and optimization the design parameters.

A lot of studies were made to predict the heat transfer rate, to evaluate performance, to find out optimal design of heat exchangers that were the fundamental component of refrigeration systems, by ANNs methods. Vega, Sen, Yang, & McClain (2001) investigated heat transfer rate estimations from Ann models of fin-tube heat exchangers used for refrigeration applications. In that study it was seen that the ANNs methodology gives upper bound of the estimate error in heat rates for input variables that are the geometrical parameters of heat exchanger and operating conditions. Another similar study was made to evaluate performance of fin and tube condenser using neural network for only input parameters of operating conditions by Zhao, & Zhang (2010). After ANN results were compared with the experimental values, all errors of estimation had found approximately %5.

Islamoglu (2003), Xie, Wang, Zeng, & Luo (2007), Orlando, Rodriguez, & Consalter (2009) and Peng, & Link (2008) were studied that heat transfer analysis for shell-and-tube and wire-on-tube heat exchangers with experimental data by artificial neural networks approach. They recommended that ANN can be used to predict the performances of thermal systems, such as modeling heat exchangers for heat transfer analysis.

ANNs modeling of refrigeration systems has been studied from past to present by numerous investigators. Steady state ANN modeling of vapor-compression liquid chillers is presented to predict its performance by the study of Swider, Browne, Bansal, & Kecman (2001). Chiller model was developed with those input parameters that were the chilled water outlet temperature from the evaporator, the cooling water inlet temperature to condenser and the evaporator capacity. The neural network predicted the compressor work input and the coefficient of performance (COP) to within ±5%.

To predict a performance of setting up experimental refrigeration system with an evaporative condenser using the applications of ANNs was made by Ertunc, & Hosoz (2006). In order to gather data of the five input parameters, those were the evaporator load, air and water flow rates passing through the condenser and both dry and wet bulb temperatures of the air stream entering the condenser, used for training and testing ANN, testing apparatus were operated steady-state conditions. Predicting five output parameters which were the condenser heat rejection rate, refrigerant mass flow rate, compressor power, electric power input to compressor motor and COP agreed with the experimental values with mean relative errors. In this study showed that refrigeration systems could alternatively be modeled using ANNs with in a high degree of accuracy.

Another similar study was made by Yilmaz, & Atik (2007) that a series of experiments were performed in order to determine the effects of changing cooling water flow rate in a experimental setup of mechanical cooling systems on the power consumption, thermal efficiency and COP. ANNs model which had one input and four output parameters estimated performance values by using the data from experiments performed. Resultant low relative error value indicated the usability of ANNs in this study.

As seen in reviewed studies, created ANN models of refrigeration systems were trained, validated and tested by using the all datas acquired from the experimental studies. As well as this experimental technique were applied to obtain the data series of input and outputs for ANNs, in the literature was showed numerical technique that these data series of the verifying numerical model with experimental studies were attained to calculate by the commercial analysis program. The numerical method was used to determine the data series for theirs ANN models by the studies of Ayata, Cavusoglu, & Arcaklioglu (2006) and Xie, Sunden, Wang, & Tang (2009). In these studies, current model was created numerically by analysis program and then numerical model was verified with experimental values. Input and output series of the determined design parameters for the structure of ANN model were computed by confirmed numerical analysis. The outputs values of design parameters were predicted by ANN models generated from the datas of numerical analysis.

There isn't any study about that design parameters of domestic refrigerators were investigated on the distribution of temperature and air flow inside internal air volume by using ANNs method in the literature. Only one study was presented to make by Antonio, & Afonso (2011) which was predicted the air temperature fields inside the household refrigerator's cabin with using ANN method. In this study, ANN model was developed with input parameters that were the location (x, y, z coordinates) of thermocouples and its temperature values from acquired the experimental study.

As mentioned in the literature in strongly, CFD methods are very successful for determining the design parameters according to the distribution of air flow and temperature inside the household refrigerators and ANN methods are suitable for estimating the performance of refrigeration systems On the other hand, both CFD and ANN methods aren't presented to determine the feasible design of refrigerator Namely, in this thesis, unlike other studies, optimization design parameters of the domestic refrigerator was made to use the numerical and experimental investigations by the parametric and ANN methods.

CHAPTER TWO
REFRIGERATORS

2.1 History of Refrigerators Development

Before the invention of the refrigerator, icehouses were used to provide cool storage for most of the year. Placed near freshwater lakes or packed with snow and ice during the winter, they were once very common. Natural means are still used to cool foods today. On mountainsides, runoff from melting snow is a convenient way to cool drinks, and during the winter one can keep milk fresh much longer just by keeping it outdoors (http://en.wikipedia.org/wiki/Refrigerator).

In the 11th century, the Persian physicist and chemist Ibn Sina invented the refrigerated coil, which condenses aromatic vapors. This was a breakthrough in distillation technology and he made use of it in his steam distillation process, which requires refrigerated tubing, to produce essential oils.

The first known artificial refrigeration was demonstrated by William Cullen at the University of Glasgow in 1748. Between 1805, when Oliver Evans designed the first refrigeration machine that used vapour instead of liquid, and 1902 when Willis Havilland Carrier demonstrated the first air conditioner, scores of inventors contributed many small advances in cooling machinery. In-home refrigeration became a reality in 1834 with the invention of the cooling compression system by the American inventor Jacob Perkins. In 1850 or 1851, Dr. John Gorrie demonstrated an ice maker.

In 1857, Australian James Harrison developed the world first practical ice making machine and refrigeration system, and it was used in the brewing and meat packing industries of Geelong, Victoria. Ferdinand Carré of France developed a somewhat more complex system in 1859. Unlike earlier compression-compression machines, which used air as a coolant, Carré's equipment contained rapidly expanding ammonia. The absorption refrigerator was invented by Baltzar von Platen and Carl Munters from Sweden in 1922, while they were still students at the Royal Institute of Technology in Stockholm. It became a worldwide success and was commercialized by Electrolux. Other pioneers included Charles Tellier, David Boyle, and Raoul Pictet. Carl von Linde was the first to patent and make a practical and compact refrigerator.

These home units usually required the installation of the mechanical parts, motor and compressor, in the basement or an adjacent room while the cold box was located in the kitchen. There was a 1922 model that consisted of a wooden cold box, water-cooled compressor, an ice cube tray and a 0.25 m^3 compartment. In 1923 Frigidaire introduced the first self-contained unit. About this same time porcelain-covered metal cabinets began to appear. Ice cube trays were introduced more and more during the 1920s; up to this time freezing was not an auxiliary function of the modern refrigerator.

The first refrigerator to see widespread use was the General Electric Monitor-Top refrigerator introduced in 1927, so-called because of its resemblance to the gun turret on the ironclad warship USS Monitor of the 1860s. The compressor assembly, which emitted a great deal of heat, was placed above the cabinet, and surrounded with a decorative ring. Over a million units were produced. As the refrigerating medium, these refrigerators used either sulfur dioxide, which is corrosive to the eyes and may cause loss of vision, painful skin burns and lesions, or methyl formats, which is highly flammable, harmful to the eyes, and toxic if inhaled or ingested. Many of these units are still functional today. These cooling systems cannot legally be recharged with the hazardous original refrigerants if they leak or break down.

The introduction of Freon in the 1920s expanded the refrigerator market during the 1930s and provided a safer, low-toxicity alternative to previously used refrigerants. Separate freezers became common during the 1940s; the popular term at the time for the unit was a deep freeze. These devices, or appliances, did not go into mass production for use in the home until after World War II. The 1950s and 1960s saw technical advances like automatic defrosting and automatic ice making. More efficient refrigerators were developed in the 1970s and 1980s, even though environmental issues led to the banning of very effective (Freon) refrigerants. Early refrigerator models (from 1916) had a cold compartment for ice cube trays.

From the late 1920s fresh vegetables were successfully processed through freezing by the Postum Company (the forerunner of General Foods), which had acquired the technology when it bought the rights to Clarence Birdseye's successful fresh freezing methods.

The first successful application of frozen foods occurred when General Foods heiress Marjorie Merriweather Post deployed commercial-grade freezers in Spaso House, the US Embassy in Moscow, in advance of the Davies' arrival. Post, fearful of the USSR's food processing safety standards, fully stocked the freezers with products from General Foods' Birdseye unit. The frozen food stores allowed the Davies to entertain lavishly and serve fresh frozen foods that would otherwise be out of season. Upon returning from Moscow, Post directed General Foods to market frozen product to upscale restaurants.

Home freezers as separate compartments, or as separate units, were introduced in the United States in 1940. Frozen foods, previously a luxury item, began to be commonplace.

2.2 Main Refrigeration System

The main goal of a refrigeration system which performs the reverse effect of a heat engine is to remove the heat from a low-level temperature medium (heat source) and to transfer this heat to a higher level temperature medium (heat sink). Figure 2.1 shows a thermodynamic system acting as refrigeration machine. The absolute temperature of the source is T_L and the heat transferred from the source is the refrigeration effect (refrigeration load) Q_L. On the other side, the heat rejection to the sink at the temperature T_H is Q_H . Both effects are accomplished by the work input

W. For continuous operation, the first law of thermodynamics is applied to the system (Dincer & Kanoglu, 2010).

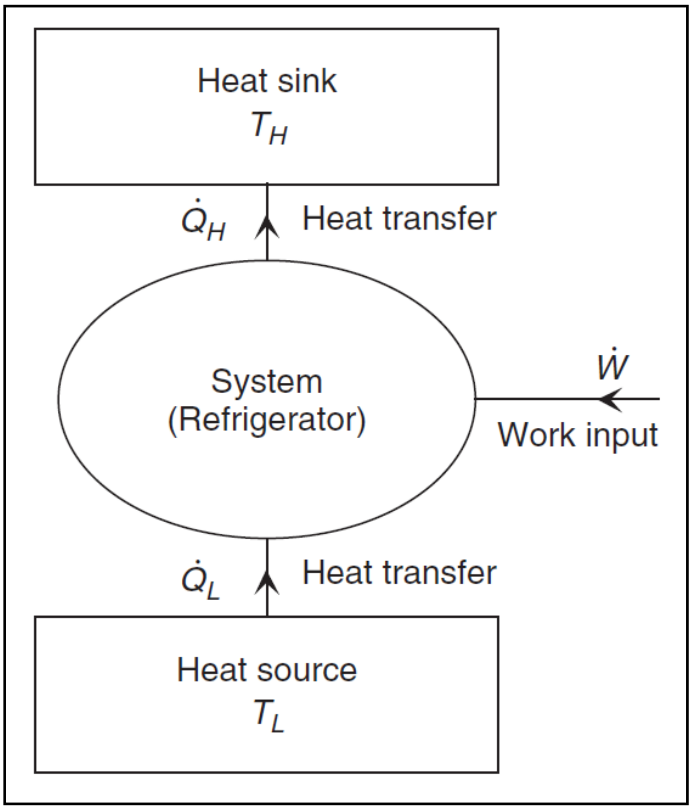

Figure 2.1 A thermodynamic system acting as a refrigerator (Dincer & Kanoglu, 2010)

Refrigeration is one of the most important thermal processes in various practical applications, ranging from space conditioning to food cooling. In these systems, the refrigerant is used to transfer the heat. Initially, the refrigerant absorbs heat because its temperature is lower than the heat source's temperature and the temperature of the refrigerant is increased during the process to a temperature higher than the heat sink's temperature. Therefore, the refrigerant delivers the heat. Refrigeration is one of the most important thermal processes in various practical applications, ranging from space conditioning to food cooling. In these systems, the refrigerant is used to transfer the heat. Initially, the refrigerant absorbs heat because its temperature is lower than the heat source's temperature and the temperature of the refrigerant is increased during the process to a temperature higher than the heat sink's temperature. Therefore, the refrigerant delivers the heat.

The main refrigeration systems and cycles that we deal with are

- vapor-compression refrigeration systems,
- absorption refrigeration systems,
- air-standard refrigeration systems,
- jet ejector refrigeration systems,
- thermoelectric refrigeration, and
- thermoacoustic refrigeration.

In domestic refrigerators, vapor-compression systems are the most commonly used refrigeration systems and each systems employs a compressor.

2.3 Domestic Refrigerators

The vapor-compression refrigerating systems used with modern refrigerators vary considerably in capacity and complexity, depending on the refrigerating application. They are hermetically sealed and normally require no replenishment of refrigerant or oil during the appliance's useful life. The components of the system must provide optimum overall performance and reliability at minimum cost. In addition, all safety requirements of the appropriate safety standard (e.g., IEC Standard 60335-2-24, UL Standard 250) must be met. The fully halogenated refrigerant R-12 was used in household refrigerators for many years. However, because of its strong ozone depletion property, appliance manufacturers have replaced R-12 with environmentally acceptable R-134a or isobutene (ASHRAE, 2006).

In household refrigerators, vapor-compression refrigeration circuit (Figure2.2) has five major components and some auxiliary equipment associated with these major components. These are compressor, condenser, evaporator, capillary tube (expansion valve) and refrigerant.

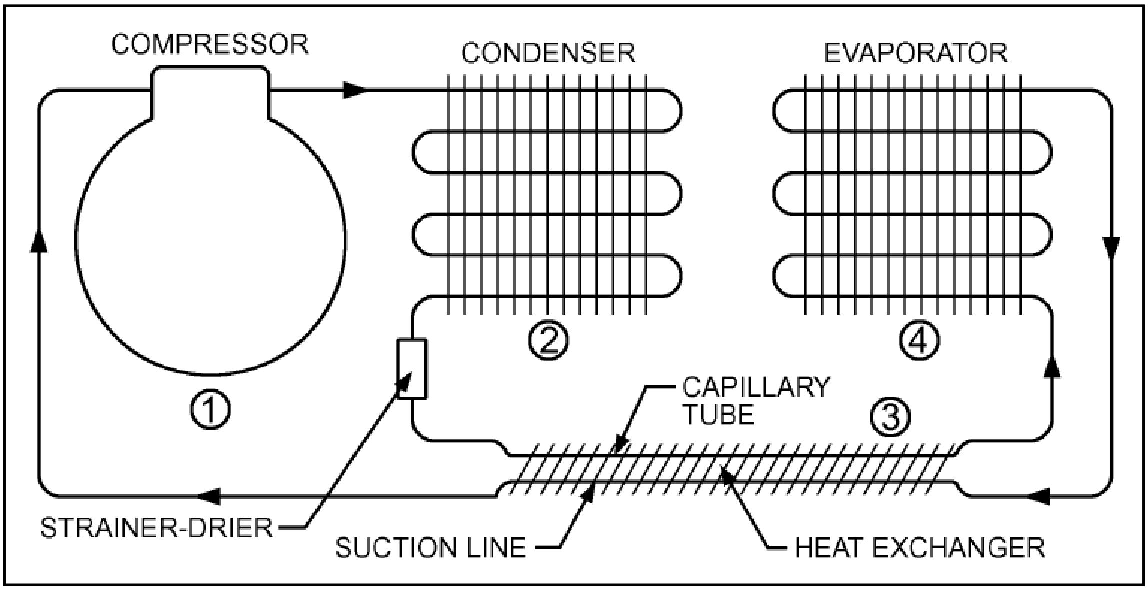

Figure 2.2 Refrigeration circuit (ASHRAE, 2006)

Figure shows a common refrigerant circuit for a vapor compression refrigerating system. In the refrigeration cycle,

1. Electrical energy supplied to the motor drives a positive displacement compressor, which draws cold, low-pressure refrigerant vapor from the evaporator and compresses it.

2. The resulting high-pressure, high-temperature discharge gas then passes through the condenser, where it is condensed to a liquid while heat is rejected to the ambient air.

3. Liquid refrigerant passes through a metering (pressure-reducing) capillary tube to the evaporator, which is at low pressure.

4. The low-pressure, low-temperature liquid in the evaporator absorbs heat from its surroundings, evaporating to a gas, which is again withdrawn by the compressor.

2.3.1 Compressor

In a refrigeration cycle, the compressor has two main functions within the refrigeration cycle. One function is to pump the refrigerant vapor from the evaporator so that the desired temperature and pressure can be maintained in the evaporator. The second function is to increase the pressure of the refrigerant vapor through the process of compression, and simultaneously increase the temperature of the refrigerant vapor. By this change in pressure the superheated refrigerant flows through the system (Dincer & Kanoglu, 2010).

Refrigerant compressors, which are known as the heart of the vapor-compression refrigeration systems, can be divided into two main categories: displacement compressors and dynamic compressors. Both displacement and dynamic compressors can be hermetic, semi hermetic or open types.

The compressor both pumps refrigerant round the circuit and produces the required substantial increase in the pressure of the refrigerant. The refrigerant chosen and the operating temperature range needed for heat pumping generally lead to a need for a compressor to provide a high pressure difference for moderate flow rates, and this is most often met by a positive displacement compressor using a reciprocating piston. Other types of positive displacement compressor use rotating vanes or cylinders or intermeshing screws to move the refrigerant. In some larger applications, centrifugal or turbine compressors are used, which are not positive displacement machines but accelerate the refrigerant vapor as it passes through the compressor housing. These various compressor types are illustrated in Figure 2.3.

In the application, there are many different types of compressors available, in terms of both enclosure type and compression system. Here are some options for evaluating the most common types:

• Reciprocating compressors are positive displacement machines, available for every application. The efficiency of the valve systems has been improved significantly on many larger models. Capacity control is usually by cylinder unloading (a method which reduces the power consumption almost in line with the capacity).

• Scroll compressors are rotary positive displacement machines with a constant volume ratio. They have good efficiencies for air conditioning and high-temperature refrigeration applications. They are only available for commercial applications and do not usually have inbuilt capacity control.

• Screw compressors are available in large commercial and industrial sizes and are generally fixed volume ratio machines. Selection of a compressor with the incorrect volume ratio can result in a significant reduction in efficiency. Part-load operation is achieved by a slide valve or lift valve unloading. Both types give a greater reduction in efficiency on part load than the reciprocating capacity control systems.

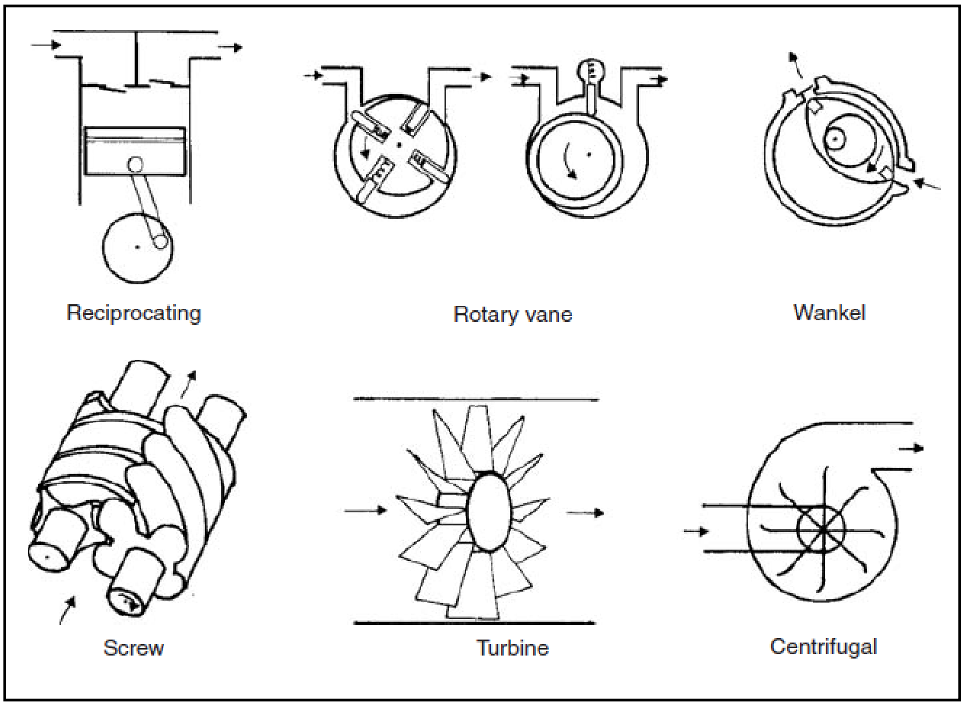

Figure 2.3 Compressor types (Dincer & Kanoglu, 2010)

The refrigerant compressors are expected to meet these requirements: high reliability, long service life, easy maintenance, easy capacity control, quiet operation, compactness and cost effectiveness.

In the selection of a proper refrigerant compressor, these criteria are considered: refrigeration capacity, volumetric flow rate, and compression rate, thermal and physical properties of refrigerant.

2.3.1.1 Hermetic Compressor

Compressors are preferable on reliability grounds to units primarily designed for the smaller range of temperatures required in household applications. In small equipment where cost is a major factor and on-site installation is preferably kept to a minimum, such as hermetically sealed motor/compressor combinations (Figure 2.4), there are no rotating seals separating motor and compressor, and the internal components are not accessible for maintenance, the casing being factory welded.

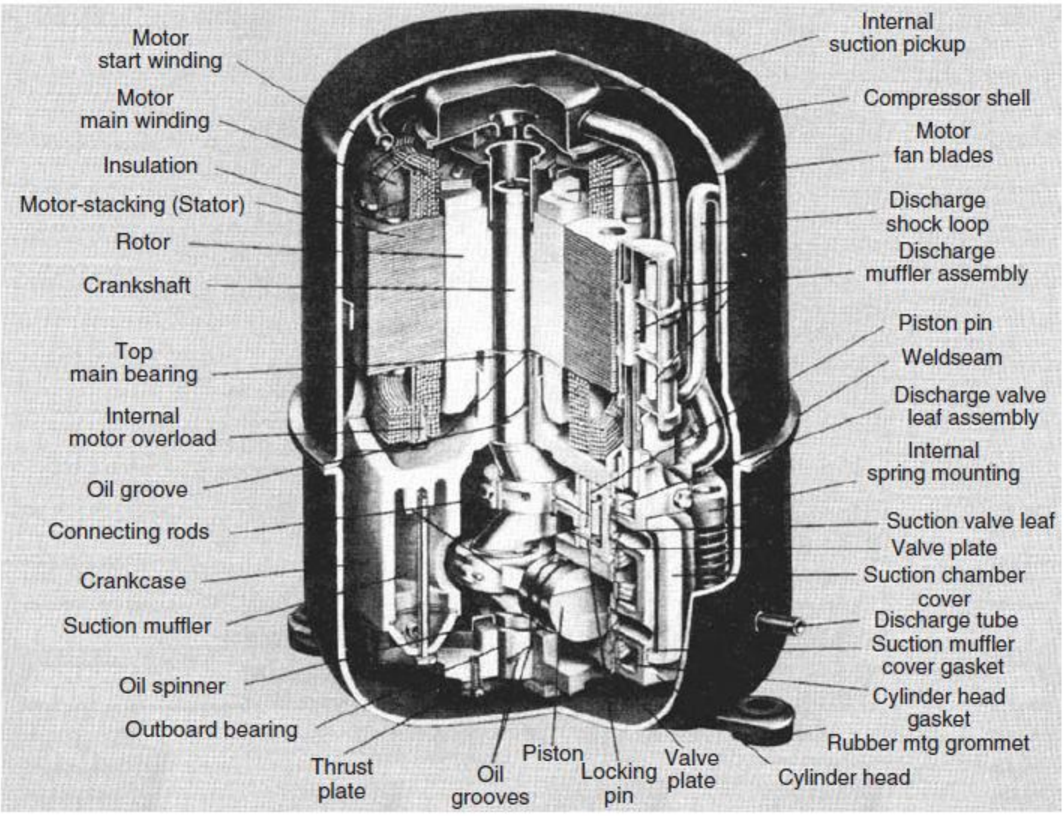

Figure 2.4 A typical hermetic reciprocating compressor (Dincer & Kanoglu, 2010)

In these compressors, which are available for small capacities, motor and drive are sealed in compact welded housing. The refrigerant and lubricating oil are contained in this housing. Almost all small motor-compressor pairs used in domestic refrigerators and freezers are of the hermetic type. An internal view of a hermetic type refrigeration compressor is shown in Figure 2.4. The capacities of these compressors are identified with their motor capacities. For example, the compressor capacity ranges from 1/12 HP to 30BG in household refrigerators. Their revolutions per minute are either 1450 or 2800 rpm. Hermetic compressors can work for a long time in small-capacity refrigeration systems without any maintenance requirement and without any gas leakage, but they are sensitive to electric voltage fluctuations, which may make the copper coils of the motor burn. The cost of these compressors is very low. Also, Figure 2.5 shows two air-cooled condensing units using a hermetic type refrigeration compressor.

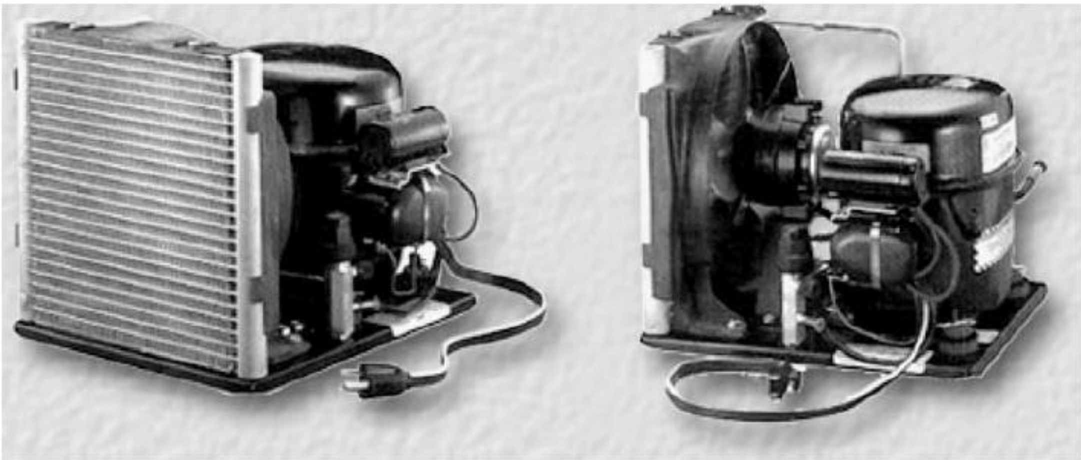

Figure 2.5 New, high-efficient compact coil air-cooled condensing units using hermetic compressors (Dincer & Kanoglu, 2010)

2.3.2 Condenser

The condenser is the main heat rejecting component in the refrigerating system. It may be cooled by natural draft on free-standing refrigerators and freezers or fan cooled on larger models and on models designed for built-in applications (ASHRAE Refrigeration, 2006).

The natural-draft (Figure 2.6) condenser is located on the back wall of the cabinet and is cooled by natural air convection under the cabinet and up the back. The most common form consists of a flat serpentine of steel tubing with steel cross wires welded on 6 mm centers on one or both sides perpendicular to the tubing. Tube-on sheet construction may also be used.

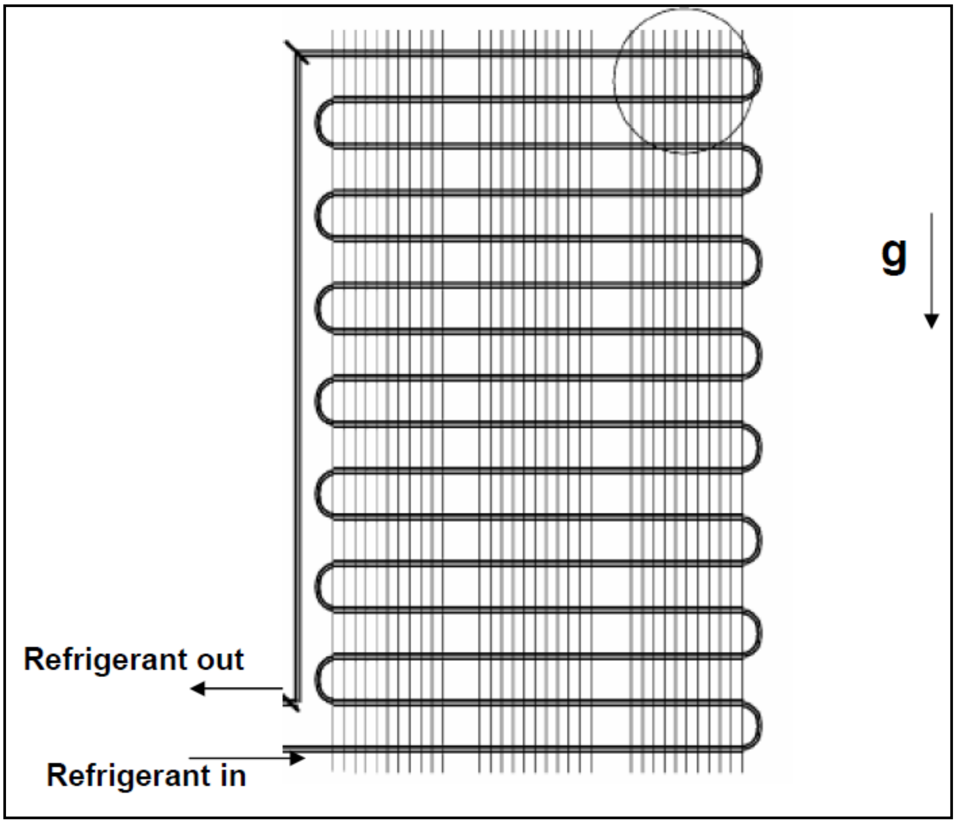

Figure 2.6. Schematic of a natural draft condenser (http://nptel.iitm.ac.in/courses/Webcourse-contents/IIT Kharagpur/Ref and Air Cond/pdf/R&AC Lecture 22.pdf)

The hot-wall condenser, another common natural-draft arrangement, consists of condenser tubing attached to the inside surface of the cabinet shell. The shell thus acts as an extended surface for heat dissipation. With this construction, external sweating is seldom a problem.

The forced-draft condenser (Figure 2.7) may be of fin-and-tube, folded banks of tube-and-wire, or tube-and-sheet construction. Various forms of condenser construction are used to minimize clogging caused by household dust and lint. The compact, fan-cooled condensers are usually designed for low airflow rates because of noise limitations. Air ducting is often arranged to use the front of the machine compartment for entrance and exit of air. This makes the cooling air system largely independent of the location of the refrigerator and allows built-in applications.

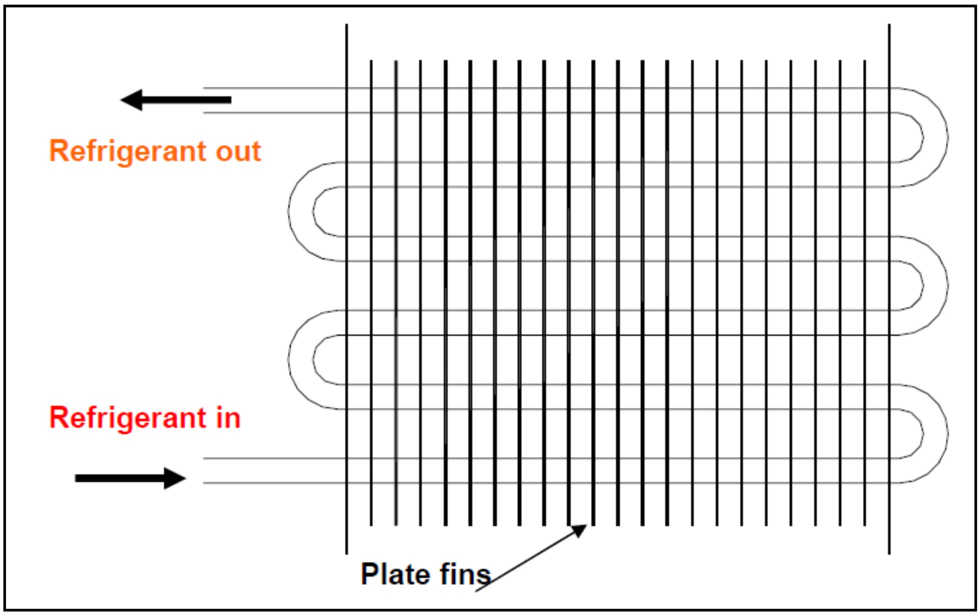

Figure 2.7 Forced convection, plate fin–and-tube type condenser (http://nptel.iitm.ac.in/courses/Webcourse-contents/IIT Kharagpur/Ref and Air Cond/pdf/R&AC Lecture 22.pdf)

For compressor cooling, the condenser may also incorporate a section where partially condensed refrigerant is routed to an oil cooling loop in the compressor. Here, liquid refrigerant, still at high pressure, absorbs heat and is re-evaporated. The vapor is then routed through the balance of the condenser, to be condensed in the normal manner.

Condenser performance may be evaluated directly on calorimeter test equipment similar to that used for compressors. However, final condenser design must be determined by performance tests on the refrigerator under a variety of operating conditions.

Generally, the most important design requirements for a condenser include sufficient heat dissipation at peak-load conditions; refrigerant holding capacity that prevents excessive pressures during pull down or in the event of a restricted or plugged capillary tube; good refrigerant drainage to minimize refrigerant trapping in the bottom of loops in low ambient, off-cycle losses, and the time required to equalize system pressures; an external surface that is easily cleaned or designed to avoid dust and lint accumulation; a configuration that provides adequate evaporation of defrost water; and an adequate safety factor against bursting.

2.3.3 Evaporator

The refrigerant undergoes various changes throughout the vapor compression cycle and it is in the evaporator where it actually produces the cooling effect. The evaporator is usually a closed insulated space where the refrigerant absorbs heat from the substance or food to be cooled (ASHRAE, 2006).

For smaller household refrigerating systems there are three types of evaporators: manual defrost evaporator, cycle defrost evaporator and frost-free evaporator.

The manual defrost evaporator is usually a box with three or four sides refrigerated. Refrigerant may be carried in tubing brazed to the walls of the box, or the walls may be constructed from double sheets of metal that are brazed or metallurgical bonded together with integral passages for the refrigerant. In this construction, the walls are usually aluminum, and special attention is required to avoid contamination of the surface with other metals that would promote galvanic corrosion and configurations that may be easily punctured during use

The cycle defrost evaporator (Figure 2.8) for the fresh food compartment is designed for natural defrost operation and is characterized by its low thermal capacity. It may be either a vertical plate, usually made from bonded sheet metal with integral refrigerant passages, or a serpentine coil with or without fins. In either case, the evaporator should be located near the top of the compartment and be arranged for good water drainage during the defrost cycle. In some designs, this cooling surface is located in an air duct remote from the fresh food space, with air circulated continuously by a small fan.

Figure 2.8 Cycle defrost evaporator
(http://www.brighthub.com/engineering/mechanical/articles/61270.aspx)

The frost-free evaporator (Figure 2.9) is usually a forced-air fin-and-tube arrangement designed to minimize frost accumulation, which tends to be relatively rapid in a single-evaporator system. The coil is usually arranged for airflow parallel to the fins' long dimension.

Fins may be more widely spaced at the air inlet to provide for preferential frost collection and to minimize its air restriction effects. All surfaces must be heated adequately during defrost to ensure complete defrosting, and provision must be made for draining and evaporating the defrost water outside the food storage spaces. Some more efficient designs of new evaporators' types are now commonly used in the industry. They are made of aluminum with continuous rectangular fins; fin layers are press-fitted onto the serpentine bent evaporator tube. These evaporators work in counter/parallel/cross flow configuration.

Figure 2.9 Frost-free evaporator
http://www.brighthub.com/engineering/mechanical/articles/61270.
aspx?p=2)

2.3.4 Capillary Tube (Expansion Valve)

The most commonly used refrigerant metering device (expansion valve) is the capillary tube (Figure 2.10), a small-bore tube connecting the outlet of the condenser to the inlet of the evaporator. The regulating effect of this simple control device is based on the principle that a given mass of liquid passes through a capillary more readily than the same mass of gas at the same pressure. Thus, if uncondensed refrigerant vapor enters the capillary, mass flow is reduced, giving the refrigerant more cooling time in the condenser. On the other hand, if liquid refrigerant tends to back up in the condenser, the condensing temperature and pressure rise, resulting in an increased mass flow of refrigerant. Under normal operating conditions, a capillary tube gives good performance and efficiency. Under extreme conditions, the capillary either passes considerable uncondensed gas or backs liquid refrigerant well up into the condenser (ASHRAE, 2006).

Figure 2.10 Capillary tube
http://www.brighthub.com/engineering/mechanical/articles/58420.aspx)

A capillary tube has the advantage of extreme simplicity and no moving parts. It also lends itself well to being soldered to the suction line for heat exchange purposes. This positioning prevents sweating of the otherwise cold suction line and increases refrigerating capacity and efficiency. Another advantage is that pressure equalizes throughout the system during the off cycle and reduces the starting torque required of the compressor motor. The capillary is the narrowest passage in the refrigerant system and the place where low temperature first occurs. For that reason, a combination strainer-drier is usually located directly ahead of the capillary to prevent it from being plugged by ice or any foreign material circulating through the system.

2.3.5 Refrigerants

Refrigerants are the working fluids in refrigeration and heat-pumping systems. They absorb heat from one area, such as an air-conditioned space, and reject it into another, such as outdoors, usually through evaporation and condensation. These phase changes occur both in absorption and mechanical vapor compression systems, but not in systems operating on a gas cycle using a fluid such as air. The design of the refrigeration equipment depends strongly on the properties of the selected refrigerant (ASHRAE, 2006).

Refrigerant selection involves compromises between conflicting desirable thermo physical properties. A refrigerant must satisfy many requirements, some of which do not directly relate to its ability to transfer heat. Chemical stability under conditions of use is an essential characteristic. Safety codes may require a nonflammable refrigerant of low toxicity for some applications. Cost, availability, efficiency, and compatibility with compressor lubricants and equipment materials are other concerns.

2.3.5.1 Classification of Refrigerants

Primary refrigerants can be classified into the following five main groups (Dincer & Kanoglu, 2010):

- Halocarbons
- Hydrocarbons (HCs)
- Inorganic compounds
- Azeotropic mixtures
- Nonazeotropic mixtures

2.3.5.1.1. Halocarbons. The halocarbons contain one or more of the three halogens – chlorine, fluorine, or bromine are widely used in refrigeration and air-conditioning systems as refrigerants. These are more commonly known by their trade names, such as Freon, Arcton, Genetron, Isotron, and Uron. In this group, the halocarbons, consisting of chlorine, fluorine, and carbon, were the most commonly used refrigerants (so-called *chlorofluorocarbons, CFCs*). CFCs were commonly used as refrigerants, solvents, and foam-blowing agents. The most common CFCs have been CFC-11 or R-11, CFC-12 or R-12, CFC-113 or R-113, CFC-114 or R-114, and CFC-115 or R-115. Their use rapidly decreased, because of their environmental impact.

2.3.5.1.2 Hydrocarbons. HCs are the compounds that mainly consist of carbon and hydrogen. HCs include methane, ethane, propane, cyclopropane, butane, and cyclopentane. Although HCs are highly flammable, they may offer advantages as alternative refrigerants because they are inexpensive to produce and have zero ozone depletion potential (ODP), very low global warming potential (GWP), and low toxicity.

For refrigeration applications, a number of HCs such as methane (R-50), ethane (R-170), propane (R-290), *n*-butane (R-600), and isobutane (R-600a) that are suitable as refrigerants can be used.

2.3.5.1.3 Inorganic Compounds. In spite of the early invention of many inorganic compounds, today they are still used in many refrigeration, air conditioning, and heat pump applications as refrigerants. Some examples are ammonia (NH3), water (H2O), air (0.21O2 + 0.78N2 + 0.01Ar), carbon dioxide (CO2), and sulfur dioxide (SO2). Among these compounds, ammonia has received the greatest attention for practical applications

2.3.5.1.4 Azeotropic Mixtures. An azeotropic refrigerant mixture consists of two substances having different properties but behaving as a single substance. The two substances cannot be separated by distillation. The most common azeotropic refrigerant is R-502. Its COP is higher than that of R-22 and its lesser toxicity provides an opportunity to use this refrigerant in household refrigeration systems and the food refrigeration industry. Some other examples of azeotropic mixtures are R 500, R-503 and R-504.

2.3.5.1.5 Nonazeotropic Mixtures. Nonazeotropic mixture is a fluid consisting of multiple components of different volatiles that, when used in refrigeration cycles, change composition during evaporation (boiling) or condensation. Recently, nonazeotropic mixtures have been called zeotropic mixtures or blends. The application of nonazeotropic mixtures as refrigerants in refrigeration systems has been proposed since the beginning of the twentieth century. A great deal of research on these systems with nonazeotropic mixtures and on their thermo physical properties has been done since that time. Great interest has been shown in nonazeotropic mixtures, especially for heat pumps, because their adaptable composition offers a new dimension in the layout and design of vapor-compression systems. Much work has been done since the first proposal to use these fluids in heat pumps. Through the energy crises in the 1970s, nonazeotropic mixtures became more attractive in research and development on advanced vapor-compression heat pump systems.

For domestic refrigerators, R-600 (n-butane) and R134a are suitable as refrigerants can be used.

2.4 Domestic Refrigerating System Basics and Theories

2.4.1 The Ideal Vapor-Compression Refrigeration Cycle

Many of the impracticalities associated with the reversed Carnot cycle can be eliminated by vaporizing the refrigerant completely before it is compressed and by replacing the turbine with a throttling device, such as an expansion valve or capillary tube. The cycle that results is called the ideal vapor-compression refrigeration cycle, and it is shown schematically and on a *T-s* diagram in Figure 2-11. The vapor compression refrigeration cycle is the most widely used cycle for refrigerators, air conditioning systems, and heat pumps. It consists of four processes (Cengel & Boles, 2006):

- 1-2 Isentropic compression in a compressor
- 2-3 Constant-pressure heat rejection in a condenser
- 3-4 Throttling in an expansion device
- 4-1 Constant-pressure heat absorption in an evaporator

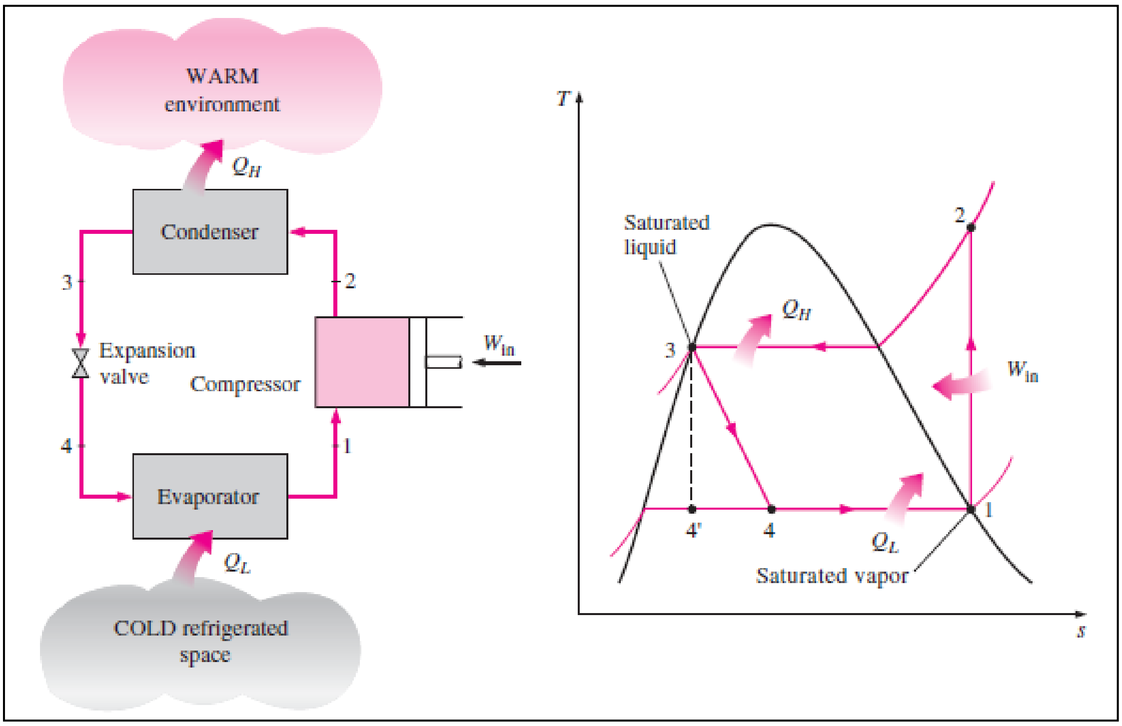

Figure 2.11 Schematic T-*s* diagram for the ideal vapor-compression refrigeration cycle (Cengel & Boles, 2006)

In an ideal vapor-compression refrigeration cycle, the refrigerant enters the compressor at state 1 as saturated vapor and is compressed isentropically to the condenser pressure. The temperature of the refrigerant increases during this isentropic compression process to well above the temperature of the surrounding medium. The refrigerant then enters the condenser as vapor at state 2 and leaves as saturated liquid at state 3 as a result of heat rejection to the surroundings. The temperature of the refrigerant at this state is still above the temperature of the surroundings.

The saturated liquid refrigerant at state 3 is throttled to the evaporator pressure by passing it through an expansion valve or capillary tube. The temperature of the refrigerant drops below the temperature of the refrigerated space during this process. The refrigerant enters the evaporator at state 4 as a low-quality saturated mixture, and it completely evaporates by absorbing heat from the refrigerated space. The refrigerant leaves the evaporator as saturated vapor and reenters the compressor, completing the cycle.

In a household refrigerator (Figure 2.12), the tubes in the freezer compartment where heat is absorbed by the refrigerant serves as the evaporator. The coils behind the refrigerator, where heat is dissipated to the kitchen air, serve as the condenser.

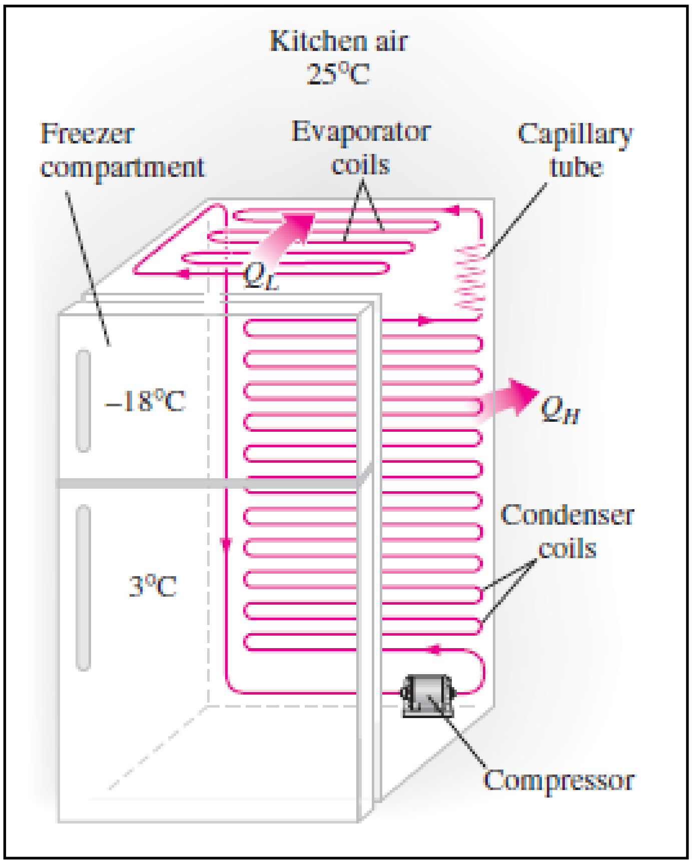

Figure 2.12 An ordinary household refrigerator (Cengel & Boles, 2006)

The area under the process curve 4-1 represents the heat absorbed by the refrigerant in the evaporator, and the area under the process curve 2-3 represents the heat rejected in the condenser. A rule of thumb is that the COP improves by 2 to 4 percent for each °C the evaporating temperature is raised or the condensing temperature is lowered.

Another diagram frequently used in the analysis of vapor-compression refrigeration cycles is the *P-h* diagram, as shown in Figure 2.13. On this diagram, three of the four processes appear as straight lines, and the heat transfer in the condenser and the evaporator is proportional to the lengths of the corresponding process curves.

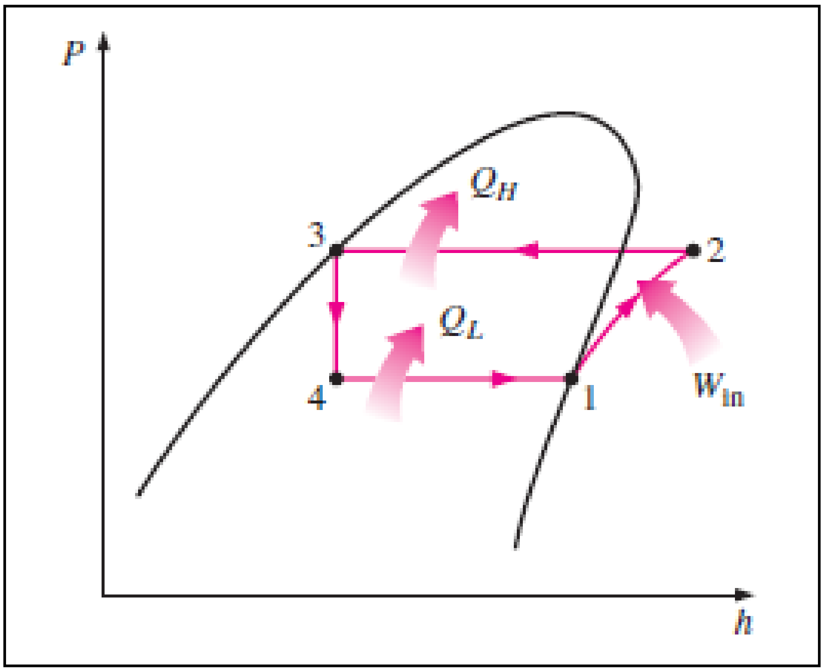

Figure 2.13 The P-*h* diagram of an ideal vapor-compression refrigeration cycle (Cengel & Boles, 2006)

The ideal vapor compression refrigeration cycle is not an internally reversible cycle since it involves an irreversible (throttling) process. This process is maintained in the cycle to make it a more realistic model for the actual vapor-compression refrigeration cycle. If the throttling device were replaced by an isentropic turbine, the refrigerant would enter the evaporator at state 4' instead of state 4. As a result, the refrigeration capacity would increase (by the area under process curve 4'-4 in Figure 2.11) and the net work input would decrease (by the amount of work output of the turbine). Replacing the expansion valve by a turbine is not practical, however, since the added benefits cannot justify the added cost and complexity.

All four components associated with the vapor-compression refrigeration cycle are steady-flow devices, and thus all four processes that make up the cycle can be analyzed as steady-flow processes. The kinetic and potential energy changes of the refrigerant are usually small relative to the work and heat transfer terms, and therefore they can be neglected. Then the steady flow energy equation on a unit–mass basis reduces to

$$(q_{in} - q_{out}) + (w_{in} - w_{out}) = h_e - h \qquad \text{... (2.1)}$$

The condenser and the evaporator do not involve any work, and the compressor can be approximated as adiabatic. Then the COPs of refrigerators and heat pumps operating on the vapor-compression refrigeration cycle can be expressed as

$$COP_R = \frac{q_L}{w_{net,in}} = \frac{h_1 - h_4}{h_2 - h_1} \qquad \text{... (2.2)}$$

$$COP_{HP} = \frac{q_H}{w_{net,in}} = \frac{h_2 - h_3}{h_2 - h_1} \qquad \text{... (2.3)}$$

where $h_1 = h_{g@P1}$ and $h_3 = h_{g@P3}$ for ideal case.

2.4.2 Actual Vapor-Compression Refrigeration Cycle

An actual vapor-compression refrigeration cycle differs from the ideal one in several ways, owing mostly to the irreversibilities that occur in various components. Two common sources of irreversibilities are fluid friction (causes pressure drops) and heat transfer to or from the surroundings. The *T-s* diagram of an actual vapor-compression refrigeration cycle is shown in Figure 2.14.

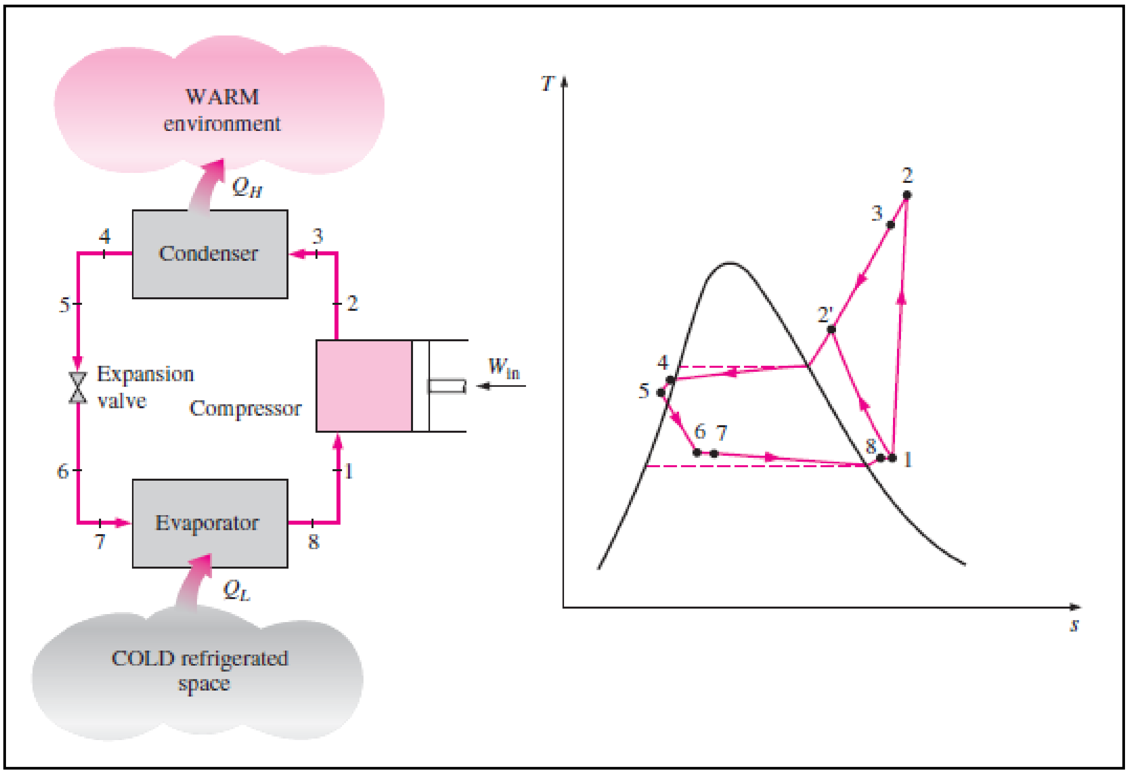

Figure 2.14 Schematic and T-*s* diagram for the actual vapor-compression refrigeration cycle (Cengel & Boles, 2006)

In the ideal cycle, the refrigerant leaves the evaporator and enters the compressor as saturated vapor. In practice, however, it may not be possible to control the state of the refrigerant so precisely. Instead, it is easier to design the system so that the refrigerant is slightly superheated at the compressor inlet. This slight overdesign ensures that the refrigerant is completely vaporized when it enters the compressor. Also, the line connecting the evaporator to the compressor is usually very long; thus the pressure drop caused by fluid friction and heat transfer from the surroundings to the refrigerant can be very significant. The result of superheating, heat gain in the connecting line, and pressure drops in the evaporator and the connecting line is an increase in the specific volume, thus an increase in the power input requirements to the compressor since steady-flow work is proportional to the specific volume.

The compression process in the ideal cycle is internally reversible and adiabatic, and thus isentropic. The actual compression process, however, involves frictional effects, which increase the entropy, and heat transfer, which may increase or decrease the entropy, depending on the direction. Therefore, the entropy of the refrigerant may increase (process 1-2) or decrease (process 1-2') during an actual compression process, depending on which effects dominate. The compression process 1-2' may be even more desirable than the isentropic compression process since the specific volume of the refrigerant and thus the work input requirement are smaller in this case. Therefore, the refrigerant should be cooled during the compression process whenever it is practical and economical to do so.

In the ideal case, the refrigerant is assumed to leave the condenser as saturated liquid at the compressor exit pressure. In reality, however, it is unavoidable to have some pressure drop in the condenser as well as in the lines connecting the condenser to the compressor and to the throttling valve. Also, it is not easy to execute the condensation process with such precision that the refrigerant is a saturated liquid at the end, and it is undesirable to route the refrigerant to the throttling valve before the refrigerant is completely condensed. Therefore, the refrigerant is subcooled somewhat before it enters the throttling valve. We do not mind this at all, however, since the refrigerant in this case enters the evaporator with a lower enthalpy and thus can absorb more heat from the refrigerated space. The throttling valve and the evaporator are usually located very close to each other, so the pressure drop in the connecting line is small.

CHAPTER THREE
NUMERICAL STUDY

3.1 Preparing Cad Model for Numerical Study

The Cad model of domestic refrigerator was taken from a white goods producer company for numerical study. Refrigerator model which has 1.7m x 0.48m x 0.45m (height x width x depth) internal dimensions has a single-door with only a fresh food cabinet (Figure 3.1.a). The cycle defrost type evaporator is located into the back wall, opposite of the door, and its area is 44.5x91 cm^2. The wire-on-tube condenser is located on the external surface of the back wall. Inner configuration of modeled refrigerator has four main glass shelves, five door shelves, two vegetable compartments and their glass shelves, a light box and a fan box (Figure 3.1.b).

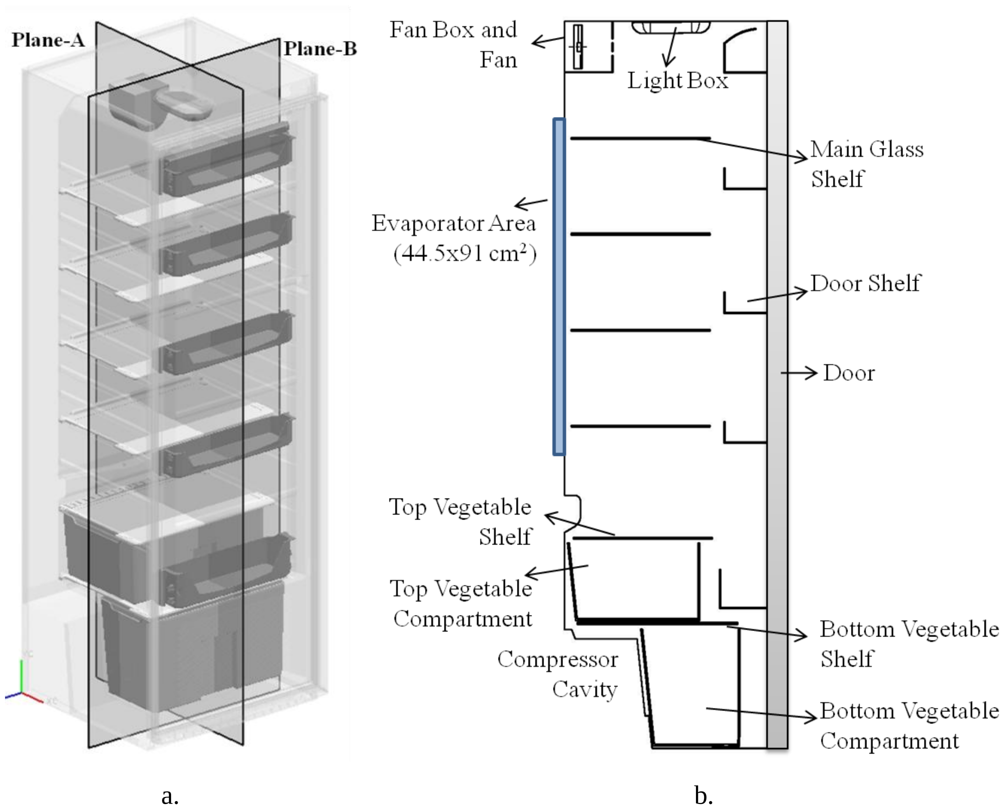

Figure 3.1 Refrigerator model views: (a) Isometric view, (b) Section of plane-A and inner configuration

These inner configurations which were assumed as a geometrical obstacle against the flow were defined a cavity inside the generated air volume. Some neglectable details of inner configuration, solid fan geometry and external walls of refrigerator (inner plastic, insulation material and sheet metal) weren't modeled for simplification. This prediction was made for having a high mesh quality and reduced the numerical analysis time.

As shown in Figure 3.2, the internal air volume of refrigerator was made up 3D model according to cad model and assumptions.

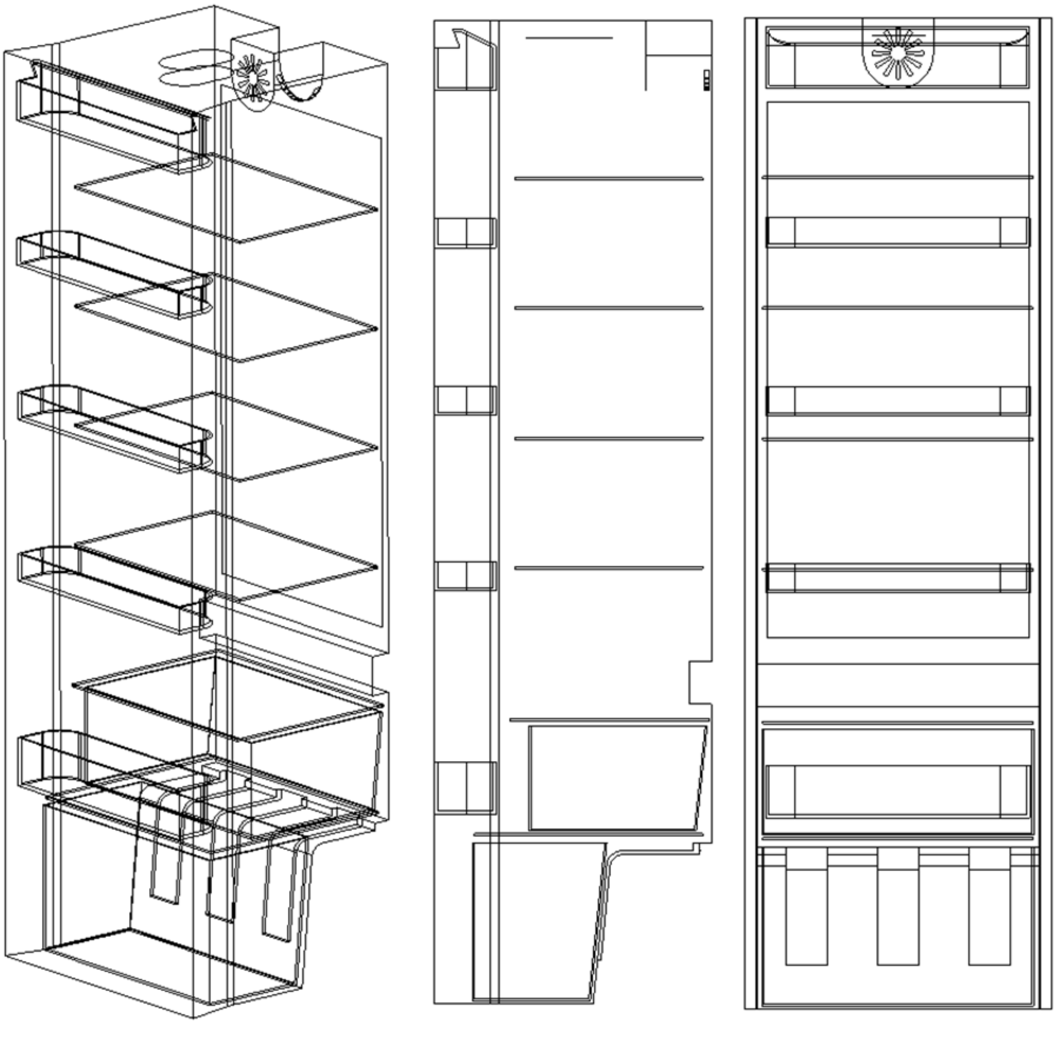

a. b. c.

Figure 3.2 Internal air volume of refrigerator model views: (a) Isometric view, (b) Left view, (c) Front view

3.2 Meshing

The most important steps to reach the closest results to real life in a Computational Fluid Dynamics (CFD) analysis are generating a proper numerical grid model and defining boundary conditions correctly. This pre-processing of the numerical study was performed at commercial CFD analysis program. The prepared computer aided design (CAD) model is imported to the package program's mesh module. Then, the names of internal air volume model's regions were defined for the ease of definitions of boundary condition.

Computational fluid dynamics require meshes that can resolve boundary layer phenomena and satisfy more stringent quality criteria than structural analyses. Because of this reason, physics preferences option is selected CFD in the mesh module. Extensive advanced mesh generation controls are available in the mesh program. Inflation control option is used for resolving the mesh on the evaporator wall regions that is located into the back wall, opposite of the door. As shown in Figure 3.3, defined inflation has five layers and mesh size growth rate is 1.01 through these layers.

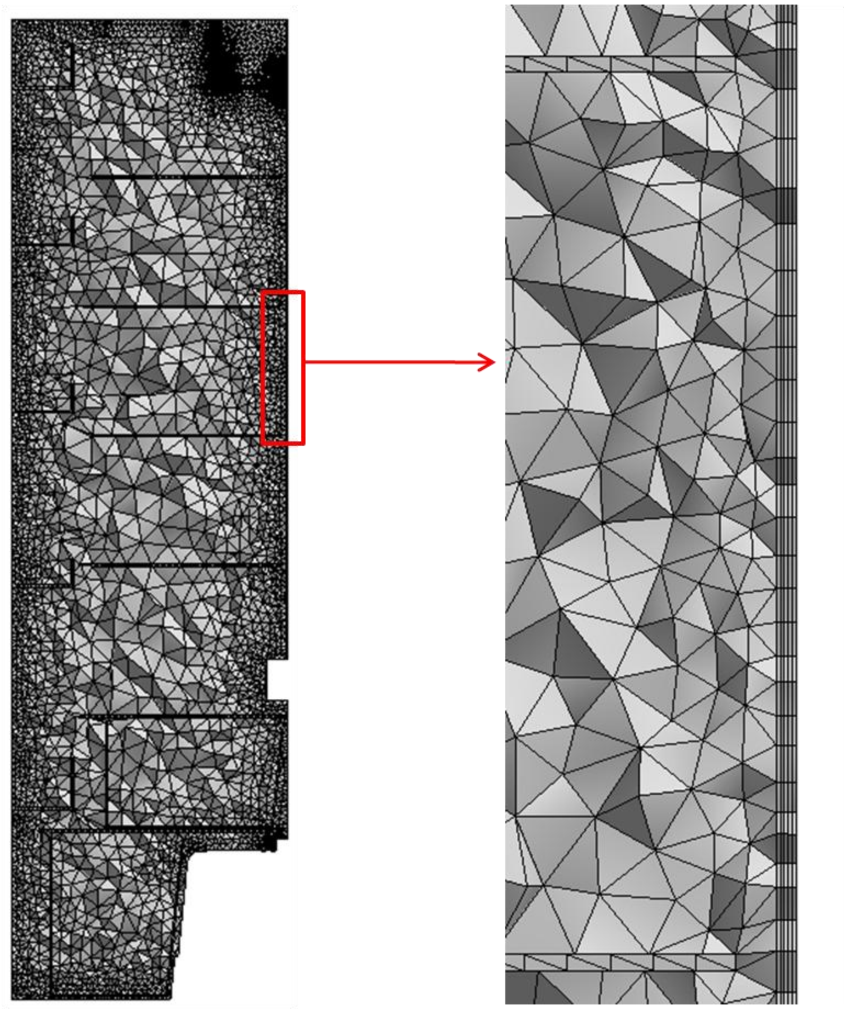

Figure 3.3 Mesh structure on the section of plane-A and inflation layer detail

Face sizing option is defined on the external walls regions for using to control mesh size. It is carried out on the fifteen external walls of internal air volume that are illustrated with colored areas in the Figure 3.4. Existing face size is 10 mm on these regions.

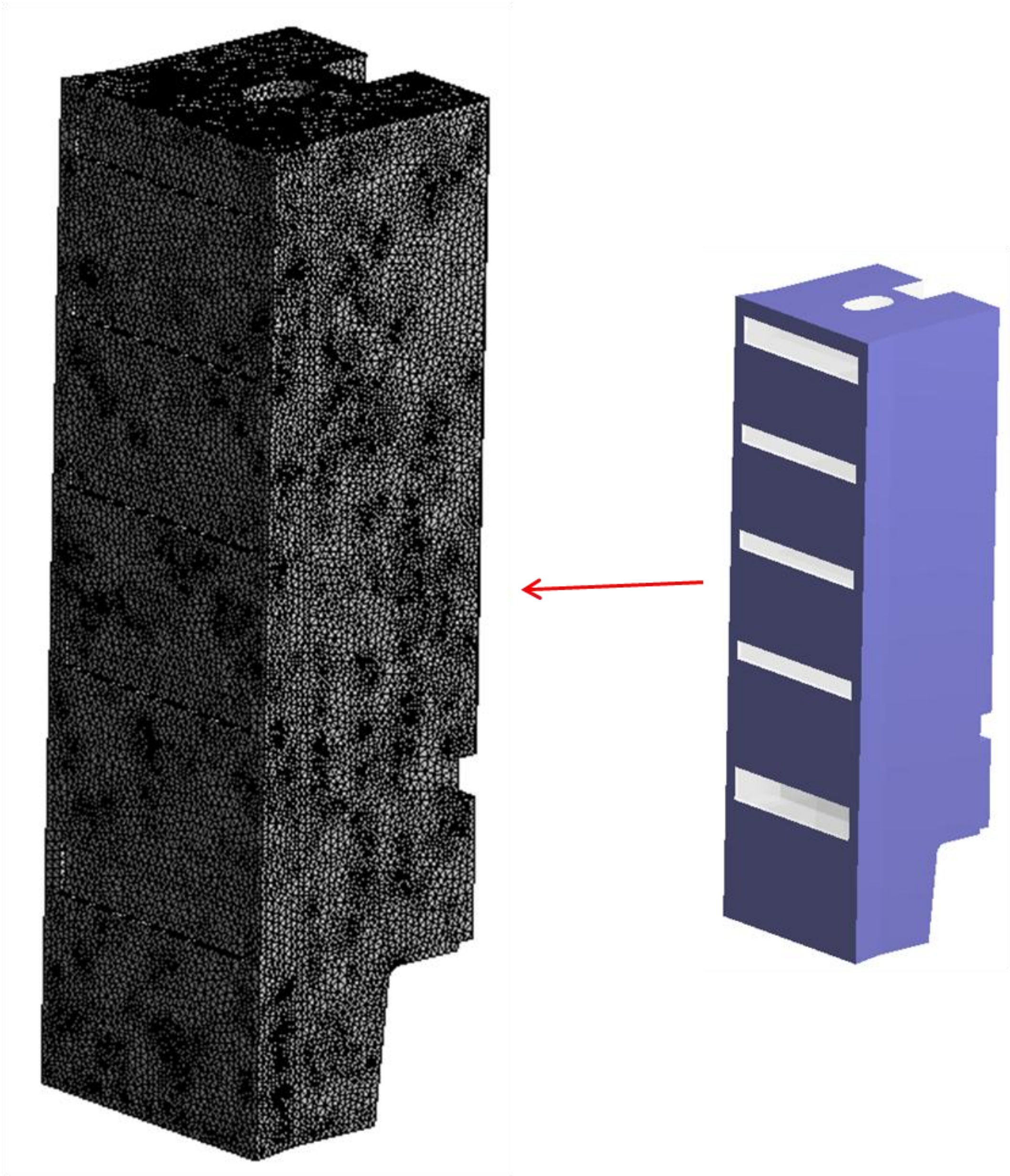

Figure 3.4 Mesh structure isometric view and existing face sizing on the external walls

The created internal air volume’s model composed of 682443 tetrahedral elements and 148785 nodes according to the previous executed mesh studies.

3.3 Boundary Conditions

The prepared numerical model was transferred to the CFD program for the preprocessing. This numerical internal air volume's model has only one fluid (air) domain that were introduced to the program.

The domestic refrigerator analysis is a transient problem by reason of the effect of compressor on-off cycle that occurs the oscillating of temperatures of the internal air volume. Most standards and studies about refrigerator in literature considered average temperatures during equilibrium condition of refrigerator. Thereby, steady state analyses were carried out for simplifying the analysis. Average temperatures in equilibrium condition are considered for determining boundary condition and validating numerical results.

Covering of refrigerator consists of internal plastic, insulation material and sheet metal from inside to outside. Heat transfer is consistently through from layers forming these covering into refrigerator. Overall heat transfer coefficient based on the thermal resistances and measuring average temperatures of external walls from experimental studies are used for modeling this heat transfer. Calculating this coefficient considered only the insulation material's thermal resistance because of the smaller thickness of the other parts of wall compared to the insulation. Overall heat transfer coefficient (U, W/m^{2}K) was calculated by (Incropera, DeWitt, Bergman, & Lavine, 2006, p.100);

$$U = \frac{1}{\mathrm{l_y}/\mathrm{k_y}} \qquad \ldots (3.1)$$

In Equation 3.1, l_y (m) is thickness of insulation material and k_y (W/mK) is the thermal conductivity of insulation material.

The gained heat to static type domestic refrigerators is removed by evaporator surface that is a result of contact with its internal air. Evaporator's temperature oscillates between the minimum and maximum value during the equilibrium condition depending on the thermostat setting. Therefore, the temperature of evaporator surface varies with time. Evaporator surface were assumed constant wall temperature according to examined numerical studies in literature and this approach showed to give acceptable results. Consequently, the temperature of evaporator was determined fixed which calculated the average value of measurement from the thermocouples on the evaporator surfaces at the experiment.

Domestic refrigerator was placed on the polystyrene plate in the test room at experiment. So heat transfer inside the bottom wall is negligible and this wall is assumed adiabatic wall condition in analyses. Heat transfer within the shelves, vegetable compartments, fan box and light box were negligible and were assumed as adiabatic.

Determined boundary conditions in accordance with experiments and assumptions are shown in Table 3.1.

Table 3.1 Boundary conditions

Region	**Boundary Condition**
Evaporator Wall	Constant Temperature -3.16 C
Front (Door) Wall	T=24.82 C
	U=0.619 W/m^{2}K
Compressor Cavity Top Wall	T=26 C
	U=0.416 W/m^{2}K
Compressor Cavity Side Wall	T=26 C
	U=0.327 W/m^{2}K
Back Wall	T=25.47 C
	U=0.331 W/m^{2}K
Side Walls	T=24.9 C
	U=0.466 W/m^{2}K
Top Wall	T=25 C
	U=0.353 W/m^{2}K
Bottom Wall and Flow Obstaclers	Adiabatic

In the fan attached to static type domestic refrigerators, heat and flow transfer occurs with natural and forced convection at its internal air volume. Natural convection gets bouncy effects as well as forced convection eventuates with the measured inlet velocities by experiment from the fan box region to air volume. These measured velocities were determined as inlet boundary conditions to the program.

The internal air's thermo physical properties according to its film temperature 3.75 C such as density (ρ), specific heat (C_p), thermal conductivity (k), thermal diffusivity (α), kinematic viscosity (ν) were shown in the Table 3.2.

Table 3.2 The internal air's thermo physical properties

T_f (K)	ρ (kg/m^3)	C_p (J/kgK)	k (W/mK)	α (m^2/s)	ν (m^2/s)
276.9	1.269	1006.538	0.024	1.94508 x10^{-5}	1.38341 x10^{-5}

In the study of Laguerre, Amara, Moureh & Flick (2007), they obtained the erroneous results for the static type refrigerator analysis without considering the effects of radiation. So, these effects of the radiation between the internal surfaces were considered.

Finally, CFD and heat transfer analysis of the modeled 3D mesh structure of internal air volume was made the following circumstances; steady state, the acceptance of laminar flow, the effects of natural, forced convection and radiation.

3.4 Solver

After the definitions of boundary conditions (material types, defined domain, temperature, heat transfer mechanisms, etc.) and initial conditions, solver control definitions were made.

Three dimensional, steady-state analyses' iterations have continued until residuals reach $10{*}E^{-3}$ and domain H-energy imbalances come below % 0.01. This took 8 hours with 8346 iterations. Heat transfer, momentum and mass and H-energy imbalances were shown in Figure 3.5, 3.6 and 3.7.

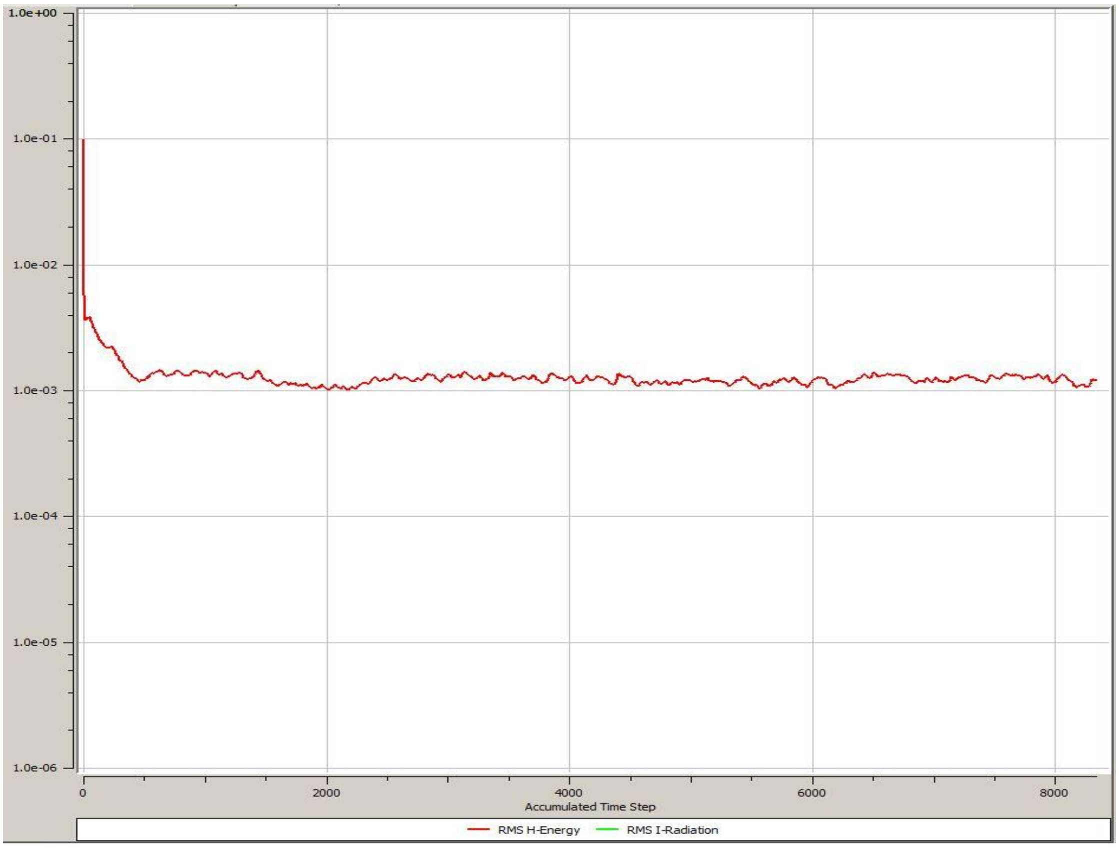

Figure 3.5 Heat transfer residuals

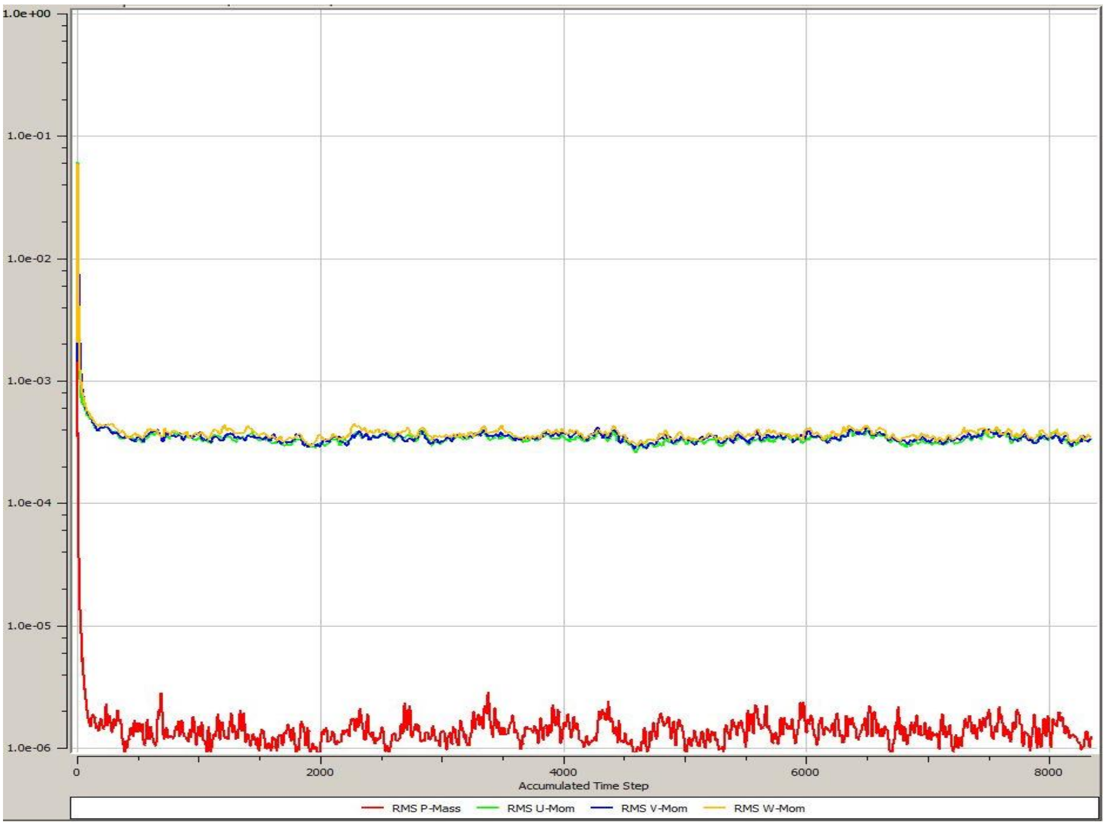

Figure 3.6 Momentum and mass residuals

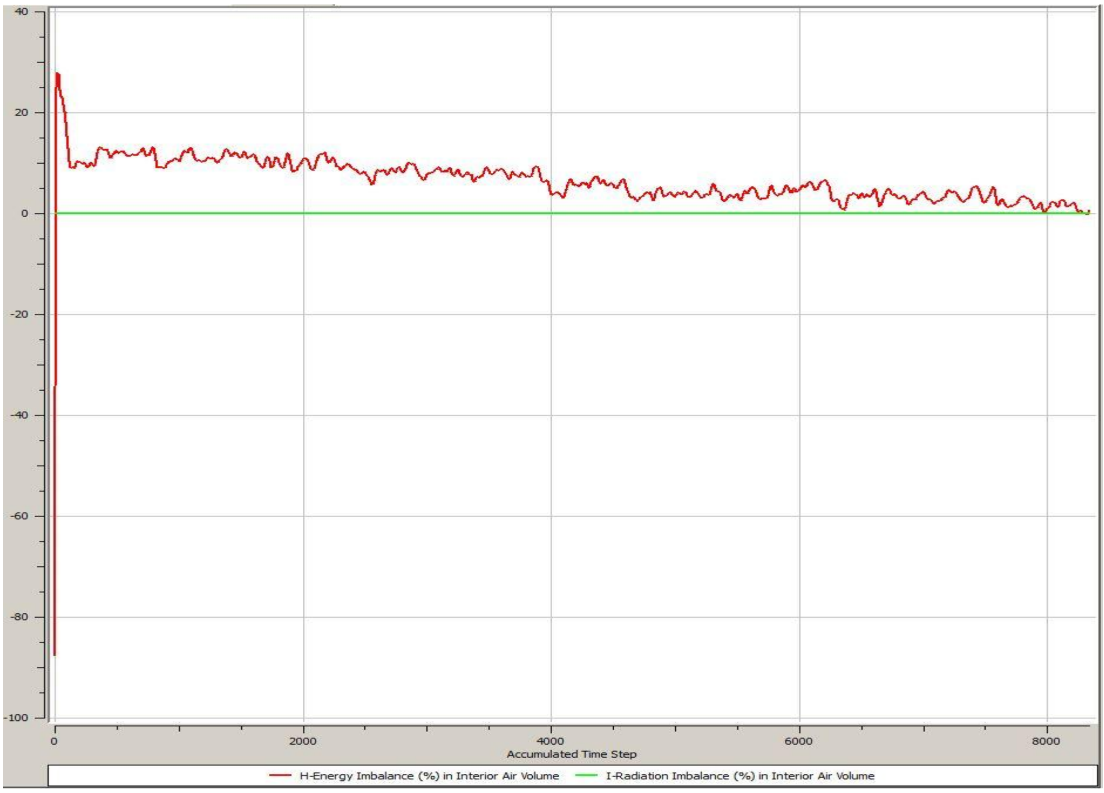

Figure 3.7 H-energy imbalance

Heat transfer and flow analyzes were made through the governing equations from the computational fluid dynamics package program solver tool.

After solution was converged; temperature contours and velocity vectors were displayed for visual consideration of the results. Calculating probes' temperatures which were located to arrangement of the thermocouples in the experiment would be compared with experimental results for using the accuracy of numerical model.

CHAPTER FOUR
PARAMETRIC STUDY

In the previous chapter, a single door static type domestic refrigerator with an only refrigerated compartment was analyzed by the computational fluid dynamics and heat transfer (CFDHT) method. The accuracy of the numerical results will be confirmed by compared with the results of experimental study in this chapter. Then, the inner design parameters will be determined by using with numerical thermal and velocity distribution results. The parametric study will be carried out in order to investigate the effects of the determined inner design parameters on the domestic refrigerator.

4.1 Experimental Study

Experimental studies are a method that should be done to testify the accuracy of the numerical model. Surface temperatures of boundary conditions and internal air temperatures were carried out to determine two separate experimental tests. The experiments were operated in the calibrated conditions of 25 C temperatures and 50% relative humidity of the test room that belonging to commercial refrigerator manufacturer.

Location of the thermocouples in the experiment setup is as shown in Figure 4.1. Figure 4.1.a shows the test setup for determining surface temperatures and Figure 4.1.b indicates the test setup in order to measure internal air temperatures. In both experiments were used twelve thermocouples.

When the refrigerator got in the thermal equilibrium with ambient, measurements was started and it had been continued twelve hour after the time of reaching steady state the refrigerator. Datas were recorded to measure the thermocouple temperature once in a second during the experiment. Average temperature value of each thermocouple was calculated by using the measured datas after reaching the steady state. The acquired internal air temperatures were used to confirm numerical analysis results.

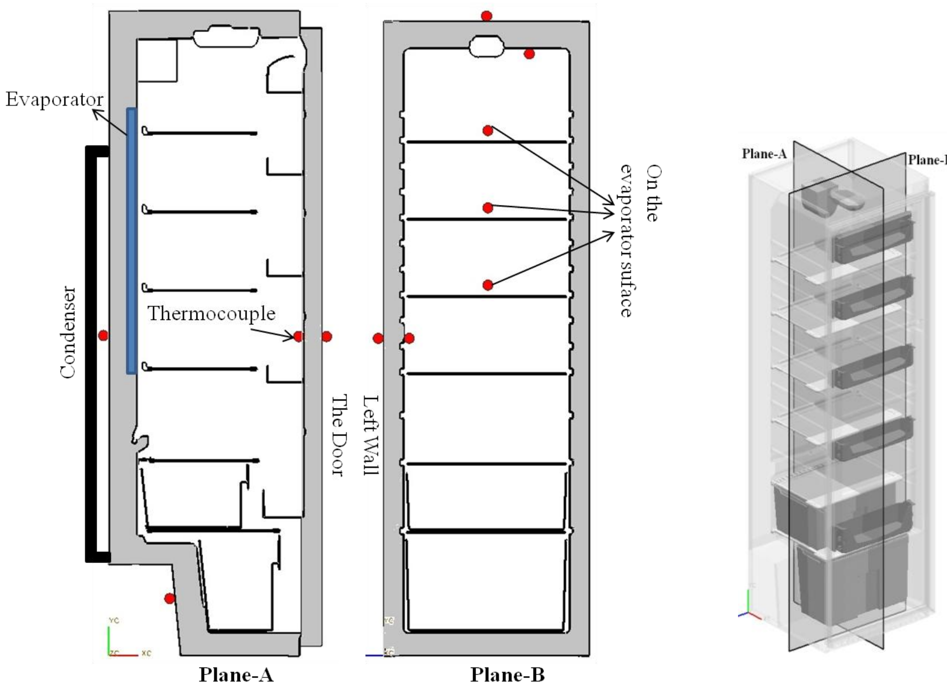

a.

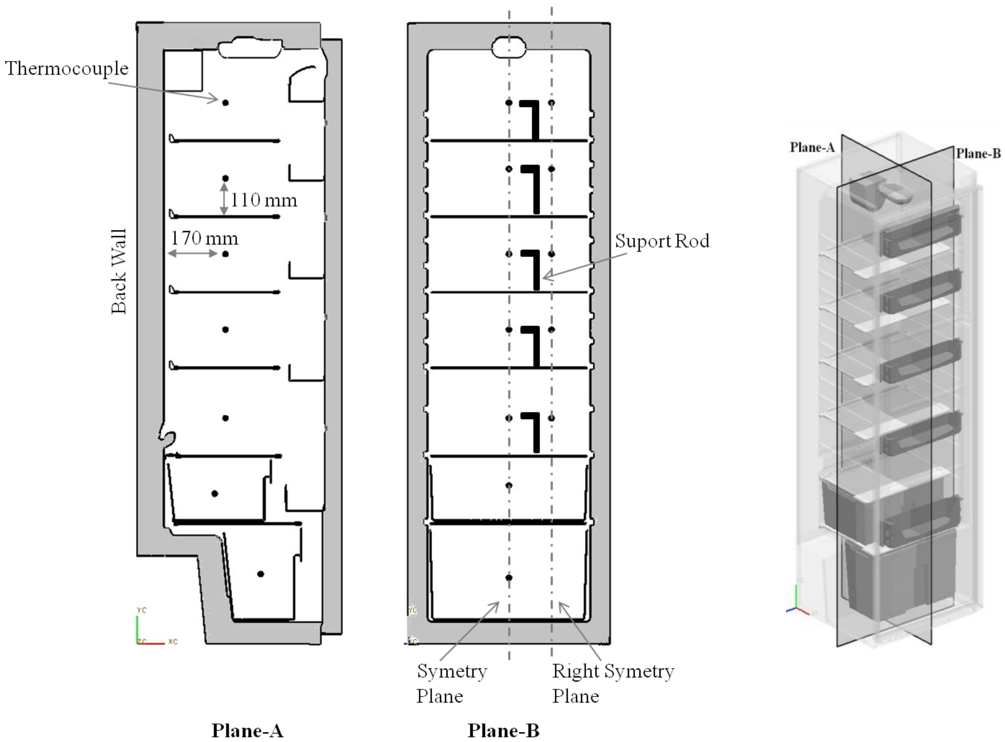

b.

Figure 4.1 Arrangement of thermocouples: (a) On surface, (b) In internal air

4.2 Verification of Numerical Model

As a result of numerical study, the temperature values corresponding to the coordinates of the thermocouples' location were given to compare with the measured temperature values from the experimental study in Table 4.1

Table 4.1 Comparison of experimental and numerical results

Location of Measurement		Experimental Average Temperature (C)	Numerical Average Temperature (C)	Absolute Difference (C)
Glass Shelf 1 (R1)	Right	5.59	3.84	1.75
	Center	5.42	3.61	1.81
Glass Shelf 2 (R2)	Right	3.30	3.26	0.04
	Center	3.50	2.74	0.05
Glass Shelf 3 (R3)	Right	2.54	2.72	0.18
	Center	2.39	2.56	0.17
Glass Shelf 4 (R4)	Right	2.74	2.62	0.12
	Center	2.76	2.72	0.04
Glass Shelf 5 (R5)	Right	3.86	5.11	1.25
	Center	3.73	4.53	0.80
Vegetable Compartments	Top. Veg.	6.42	8.50	2.08
	Bottom Veg.	8.81	6.98	1.83

The average absolute difference is 0.84 C between experimental and numerical results. According to Table 4.1, the maximum temperature difference (~2 C) between the results occurred at top vegetable compartment. This difference is within acceptable limits, so that numerical results have been concluded to be reliable.

4.3 Determination of Design Parameters

Numerical model had been verified by experimental studies and then design parameters were selected for the parametric study. The suitability of refrigerator design was emphasized to investigate by considering the distributions of temperature and velocity. Therefore, the design parameters were determined according to acquired the distributions of temperature and velocity from the numerical results.

The temperature and flow field on the symmetry plane (Plane-A) are shown together in Figure 4.2. The colored scale points to the temperature distribution of internal air volume and the black-white vectors indicate the projections of air velocity vectors on this plane.

Considering the temperature field, the temperature values of upper regions are observed to be lower. This situation occurs with the effects of fan. The warm air at upper region is absorbed from the inlets of fan box and is blown onto the evaporator surface. So, this warm air is cooled by the forced convection. The horizontal placement of fan box on the rear wall and the average velocity of fan outlets play important role to reduce the temperature values of upper regions.

To consider of flow field that the air flows downward along the evaporator surface then it flows upward along the door surface by the natural and forced convection. High velocity values occurs the near regions of the evaporator surface. Therefore, the cooled air can reach easier to downward regions with increasing the evaporator height.

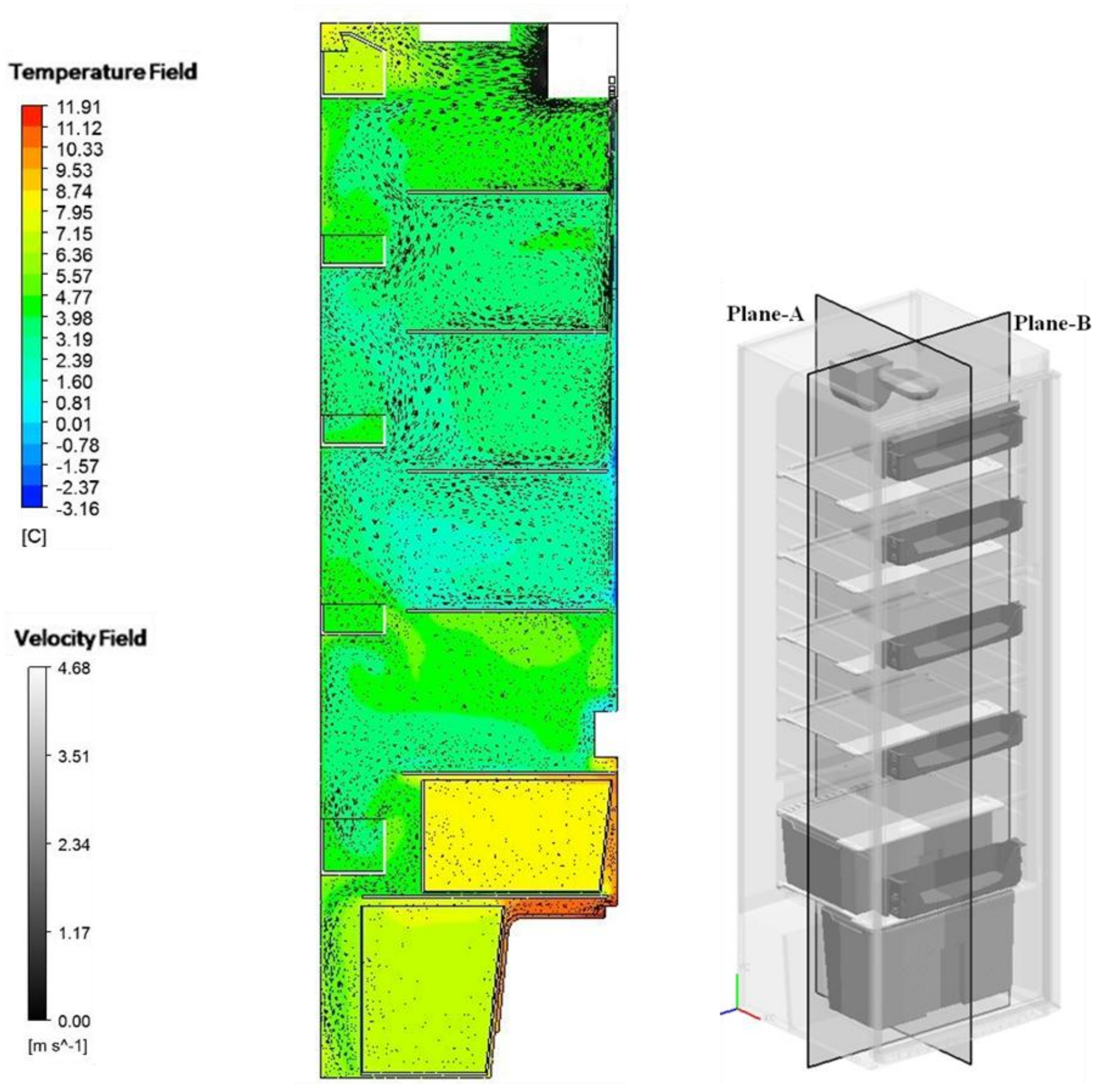

Figure 4.2 Temperature and flow field on the symmetry plane-A

To evaluate the distribution of the temperature and velocity together is shown that the cooled air on the evaporator surface moves downward and reachs to internal surfaces of refrigerator, then it moves upward to absorb heat on the internal surface. As a result, the gaps between the evaporator surface to glass shelf is determined to play an important role above the thermal uniformity in order to occur cold air flow inside the refrigerator. Otherwise, the temperature value of cold air flow was presented to depend on the evaporator’s surface temperature by Laguerre, Amara, & Flick, (2004) and Amara, Laguerre, Mojtabi, Lartigue, & Flick (2008).

Finally, the temperature of evaporator surface, the height of evaporator, the gap between evaporator surface to glass shelf, the horizontal placement of fan box on the rear wall and the average velocity of fan outlets are determined as the design parameters according to the investigation of numerical results and the literature survey in our thesis.

4.4 Implementation of Parametric Study

After the numerical studies were verified experimentally, the parametric study was made to investigate the correlation between the variation of determined design parameters and the design outputs for internal air model. In the methods of parametric study, input data which can be controlled the range of its values is applied to validating numerical model and desired output data are obtained as a result of solution. Due to increase the number of input parameters and the width of the range of its value, the required processing load and time increase proportionally for solution.

Parametric study was performed by using the parametric design section of a commercial analysis program. Input data of this study are determined five design parameters, the range of input values variation shown in Table 4.2. For the range of values given in the table, fifty different design points were created by program. These generated design points were solved with numerical analysis and output data were acquired from the analysis results.

Table 4.2 The range of design parameters values variation

Design Parameter	**Range**	**Current Value**
Evaporator Height	450 - 910 mm	910 mm
Evaporator Temperature	-8 – 0 C	-3.16 C
Gap Between Evaporator Surface to Glass Shelf	5 – 25 mm	15 mm
Average Velocity of Fan Outlets	1 - 6 m/s	3.66 m/s
Horizontal Placement of Fan Box on The Rear Wall	110 - 369.34 mm	239.67 mm

Dimension of B is the horizontal distance of the fan box center to the left wall and this dimension is 239.67 mm in the current situation, shown in Figure 4.3. Dimension of A which has the minimum value of 50 mm, is the distance of the fan box side walls to the both side walls of refrigerator. So, the fan box location is changed within the range of 110-369.34 mm horizontally.

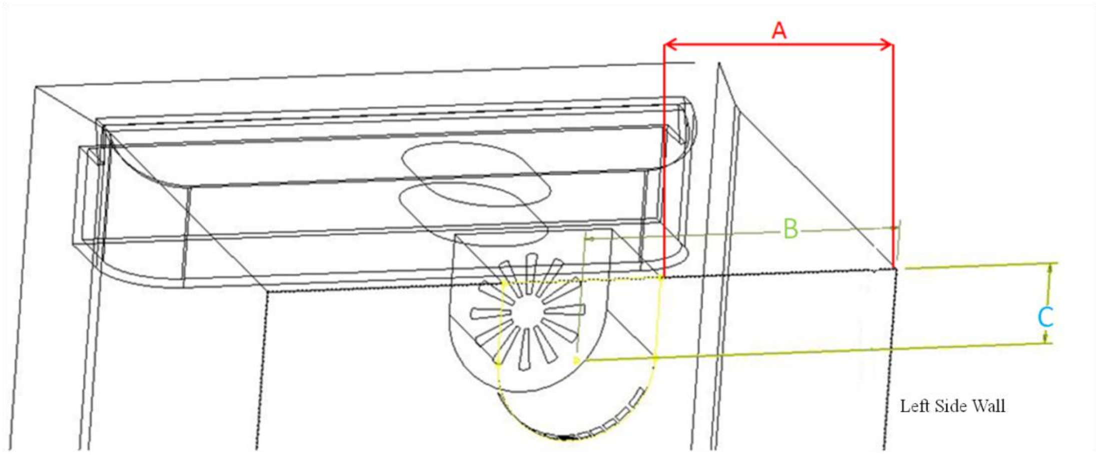

Figure 4.3 Horizontal placement of fan box on the rear wall

The temperature of three thermocouples located in the interior air volume of refrigerator according to the standard of ISO 15502, shown in Figure 4.4, and the amount of heat taken from evaporator surface (Q_{Evap}) were determined as an output data for parametric study. In reference to standard, each thermocouple temperature (T_1, T_2, T_3) must be within $0<T<10$ C and the average temperature of these thermocouples mustn't exceed up maximum 5 C. Under the restrictive conditions, five output parameters were attained that were the values of T_1, T_2, T_3, T_{Ave} and Q_{Evap}.

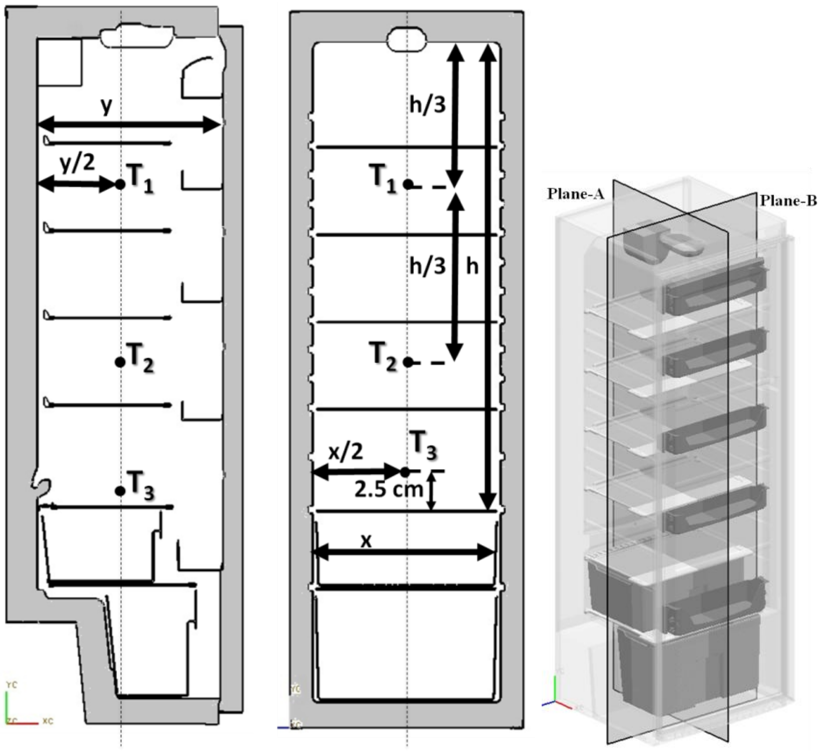

Figure 4.4 Location of thermocouples according to the standard of ISO 15502

If a different statistical methods were used instead of the parametric design section of a commercial analysis program for our parametric study, five different value of the evaporator height, five different value of the evaporator surface, five different value of the gap, five different value of average velocity of the fan outlets and five different value of the horizontal placement of fan box on the rear wall for creating a total of three thousand one hundred and twenty five different models would be had to obtain numerical solution. In addition, obtained result data of this solution had to be made interpretation by processing a statistical method. Only the duration of a model solution was considered to be approximately one hour, the solution of three thousand one hundred and twenty five models would take about 130 days when any matter didn't happen. In our thesis, a value in the determined variation range corresponding to the results of output parameters were calculated twenty one day by using the method of parametric study. Means of this method, in the improvement process of refrigerator design, the effects of changing design parameters have become possible to have an idea on the intended output data in a short time.

CHAPTER FIVE
ARTIFICIAL NEURAL NETWORKS STUDY

5.1 Fundamentals of Artificial Neural Networks

The powerful desktop computers have become commonly available, applications of artificial intelligence methods are quickly spreading too many areas of science and engineering outside the field of computer science, especially for complex systems where more traditional methods have failed to be useful. The technique of artificial neural networks (ANNs) has been shown to be particularly useful in the thermal sciences (Kreith, 2000).

The ANNs method is rooted in and inspired by the biological network of neurons in the human brain that learns from external experience, handles imprecise information, stores the essential characteristics of the external input, and generalizes previous experience. In the biological network of interconnecting neurons (Figure 5.1), each receives many input signals from other neurons and gives only one output signal which is sent to other neurons as part of their inputs. If the sum of the inputs to a given neuron exceeds a set threshold, normally determined by the electric potential of the receiver neuron which may be modified under different circumstances, the neuron fires and sends a signal to all the connected receiver neurons. If not, the signal is not transmitted. The firing decision represents the key to the learning and memory ability of the neural network.

The ANN attempts to mimic the biological neural network: the processing unit is the artificial neuron; it has synapses or interneuron connections characterized by synaptic weights; an operator performs a summation of the input signals weighted by the respective synapses; an activation function limits the permissible amplitude range of the output signal. It is also important to realize the essential difference between a biologic neural network and ANN. Biological neurons function much slower than the computer calculations associated with an artificial neuron in an ANN. On the other hand, the delivery of information across the biological neural network is much faster.

The biological one compensates for the relatively slow chemical reactions in a neuron by having an enormous number of interconnected neurons doing massively parallel processing, while the number of artificial neurons must necessarily be limited by the available hardware.

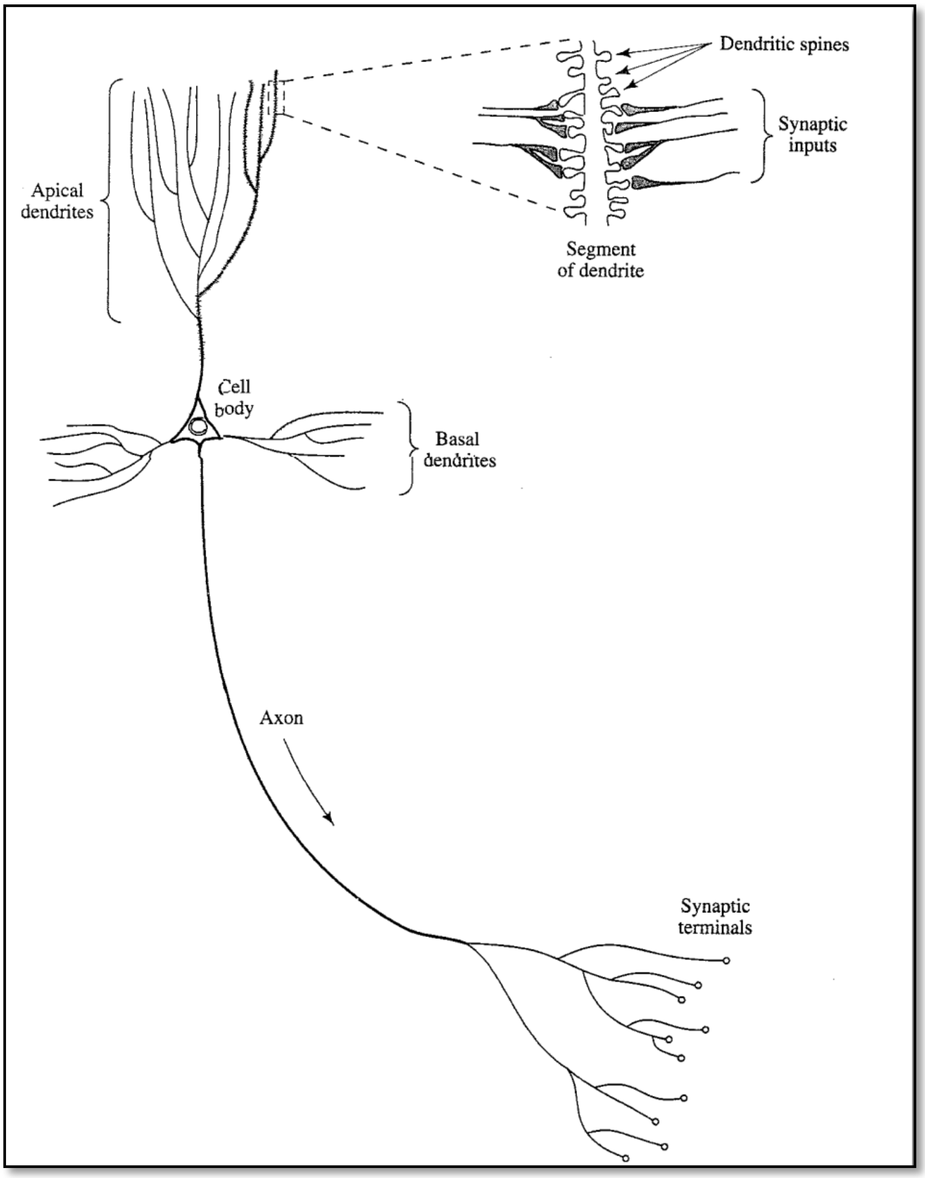

Figure 5.1 The biological cell (Haykin, 1999)

5.1.1 Methodology

Many different definitions of ANNs are possible; the one proposed is that an ANN is a network composed of a number of artificial neurons. Each neuron has an input/output characteristic and implements a local computation or function. The output of any neuron is determined by this function, its interconnection with other neurons, and external inputs. The network usually develops an overall functionality through one or more forms of training; this is the learning process. Many different network structures and configurations have been proposed, along with their own methodologies of training (Kreith, 2000).

There are many different types of ANNs, but one of the most appropriate for engineering applications is the supervised, fully connected multilayer configuration in which learning is accomplished by comparing the output of the network with the data used for training. The *feedforward* or *multilayer perceptron* is the only configuration that will be described in some detail here. Figure 5.2 shows such an ANN consisting of a series of layers, each with a number of nodes. The first and last layers are for input and output, respectively, while the others are the hidden layers. The network is said to be fully connected when any node in a given layer is connected to all the nodes in the adjacent layer.

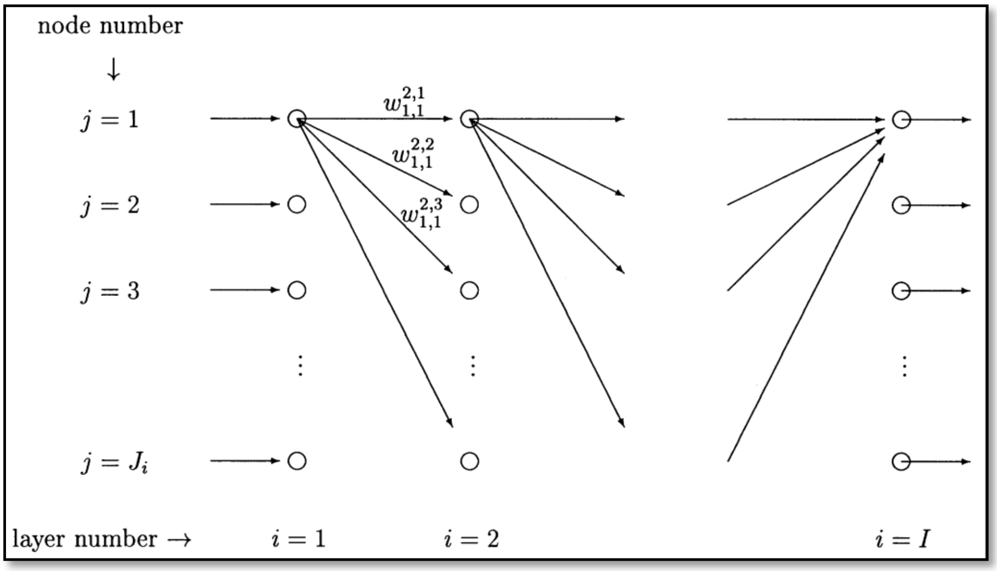

Figure 5.2 Schematic of a fully connected multilayer ANN (Kreith, 2000)

(i, j) is the jth node in the ith layer. The line connecting a node (i, j) to another node in the next layer $i + 1$ represents the synapse between the two nodes. $x_{i,j}$ is the input of the node (i, j), $y_{i,j}$ is its output, $\theta_{i,j}$ is its bias, and $w^{i,j}_{i-1,k}$ is the synaptic weight between nodes $(i - 1, k)$ and (i, j). The total number of layers, including those for input and output, is I, and the number of nodes in the ith layer is J_i. The input information is propagated forward through the network; J_1 values enter the network and J_I leave. The flow of information through the layers is a function of the computational processing occurring at every internal node in the network. The relation between the output of node $(i - 1, k)$ in one layer and the input of node (i, j) in the following layer is

$$x_{i,j} = \theta_{i,j} + \sum_{k=1}^{J_{i-1}} w^{i,j}_{i-1,k}\, y_{i-1,k} \qquad \dots (5.1)$$

Thus, the input $x_{i,j}$ of node (i, j) consists of a sum of all the outputs from the previous nodes modified by the respective internodes synaptic weights $w^{i,j}_{i-1,k}$ and a bias $\theta_{i,j}$. The weights are characteristic of the connection between the nodes and the bias of the node itself. The bias represents the propensity for the combined incoming input to trigger a response from the node and presents a degree of freedom which gives additional flexibility in the training process. Similarly, the synaptic weights are the weighting functions which determine the relative importance of the signals originated from the previous nodes.

The input and output of the node (i, j) are related by

$$y_{i,j} = \phi_{i,j}(x_{i,j}) \qquad \dots (5.2)$$

where $\phi_{i,j}(x)$, called the activation or threshold function, plays the role of the biological neuron determining whether it should fire or not on the basis of the input to that neuron. A schematic of the nodal operation is shown in Figure 5.3. It is obvious that the activation function plays a central role in the processing of information through the ANN. Keeping in mind the analogy with the biological neuron, when the input signal is small the neuron suppresses the signal altogether, resulting in a vanishing output, and when the input exceeds a certain threshold the neuron fires and sends a signal to all the neurons in the next layer. This behavior is determined by the activation function. Several appropriate activation functions have been studied. For instance, a simple step function can be used, but the presence of noncontinuous derivatives causes computing difficulties.

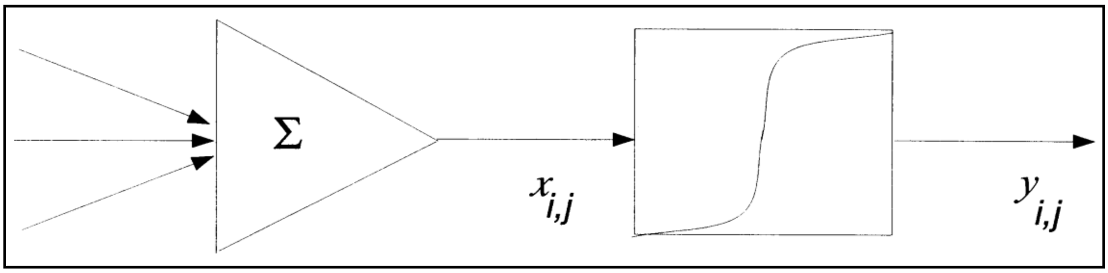

Figure 5.3 Nodal operations in an ANN (Kreith, 2000)

The most popular one is the logistic sigmoid function

$$\phi_{i,j}(\xi) = \frac{1}{1 + e^{-\frac{\xi}{c}}} \qquad \text{... (5.3)}$$

for $i > 1$, where c determines the steepness of the function. For $i = 1$, $\phi_{i,j}(\xi) = \xi$ is used instead. The sigmoid function is an approximation to the step function, but with continuous derivatives. The nonlinear nature of the sigmoid function is particularly beneficial in the simulation of practical problems. For any input $x_{i,j}$, the output of a node $y_{i,j}$ always lies between 0 and 1. Thus, from a computational point of view, it is desirable to normalize all the input and output data with the largest and smallest values of each of the data sets.

For a given network, the weights and biases must be adjusted for known input-output values through a process known as training. The backpropagation method is a widely used deterministic training algorithm for this type of ANN. The central idea of this method is to minimize an error function by the method of steepest descent to add small changes in the direction of minimization. This algorithm may be found in many recent texts on ANN and only a brief outline will be given here.

In usual complex thermal system applications where no physical models are available, appropriate training data come from experiments. The first step in the training algorithm is to assign initial values to the synaptic weights and biases in the network based on the chosen ANN configuration. The values may be either positive or negative and, in general, are taken to be less than unity in absolute value. The second step is to initiate the feedforward of information starting from the input layer. In this manner, successive input and output of each node in each layer can all be computed. When finally $i = I$, the value of $y_{I,j}$ will be the output of the network. Training of the network consists of modifying the synaptic weights and biases until the output values differ little from the experimental data which are the targets. This is done by means of the backpropagation method. First an error $\delta_{I,j}$ is quantified by

$$\delta_{I,j} = \left(t_{I,j} - y_{I,j}\right) y_{I,j} \left(1 - y_{I,j}\right) \qquad \text{... (5.4)}$$

where $t_{I,j}$ is the target output for the j-node of the last layer. The above equation is simply a finite difference approximation of the derivative of the sigmoid function. After calculating all the $\delta_{i,j}$, the computation then moves back to the layer $I - 1$. Since the target outputs for this layer do not exist, a surrogate error is used instead for this layer defined as

$$\delta_{I-1,k} = y_{I-1,k}\left(1 - y_{I-1,k}\right) \sum_{j=1}^{J_I} \delta_{I,j}\, w_{I-1,k}^{I,j} \qquad \text{... (5.5)}$$

A similar error $\delta_{i,j}$ is used for all the rest of the inner layers. These calculations are then continued layer by layer backward until layer 2. It is seen that the nodes of layer 1 have neither δ nor θ values assigned, since the input values are all known nor invariant. After all the errors $\delta_{i,j}$ are known, the changes in the synaptic weights and biases can then be calculated by the generalized delta rule:

$$\Delta w_{i-1,k}^{i,j} = \lambda \delta_{i,j} y_{i-1,k} \qquad \text{... (5.6)}$$

$$\Delta \theta_{i,j} = \lambda \delta_{i,j} \qquad \text{... (5.7)}$$

for $i < I$, from which all the new weights and biases can be determined. The quantity λ is known as the learning rate that is used to scale down the degree of change made to the nodes and connections. The larger the training rate, the faster the network will learn, but the chances of the ANN to reach the desired outcome may become smaller as a result of possible oscillating error behaviors. Small training rates would normally imply the need for longer training to achieve the same accuracy.

A cycle of training consists of computing a new set of synaptic weights and biases successively for all the experimental runs in the training data. The calculations are then repeated over many cycles while recording an error quantity E for a given run within each cycle, where

$$E = \frac{1}{2} \sum_{j=i}^{J_i} (t_{I,j} - y_{I,j})^2 \qquad \text{... (5.8)}$$

The output error of the ANN at the end of each cycle can be based on either a maximum or averaged value for a given cycle. Note that the weights and biases are continuously updated throughout the training runs and cycles. The training is terminated when the error of the last cycle, barring the existence of local minima, falls below a prescribed threshold. The final set of weights and biases can then be used for prediction purposes, and the corresponding ANN becomes a model of the input-output relation of the thermal-system problem.

5.2 Modeling Domestic Refrigerator with the ANN

The architecture of the ANN model for the domestic refrigerator which has three layers is schematically illustrated with the names of input and output parameters in Figure 5.4. The inputs to the ANN are the evaporator height (h_{Evap}), the gap between evaporator surface to glass shelf (x_{Gap}), the evaporator temperature (T_{Evap}), the average velocity of fan outlets (V_{Fan}) and the horizontal placement of fan box on the rear wall ($x_{Fan\ B.}$). The outputs from the ANN are the thermocouples temperature located by the ISO 15502 standards (T_1, T_2, and T_3), the average temperature of these thermocouples (T_{Ave}) and the evaporator heat rate (Q_{Evap}).

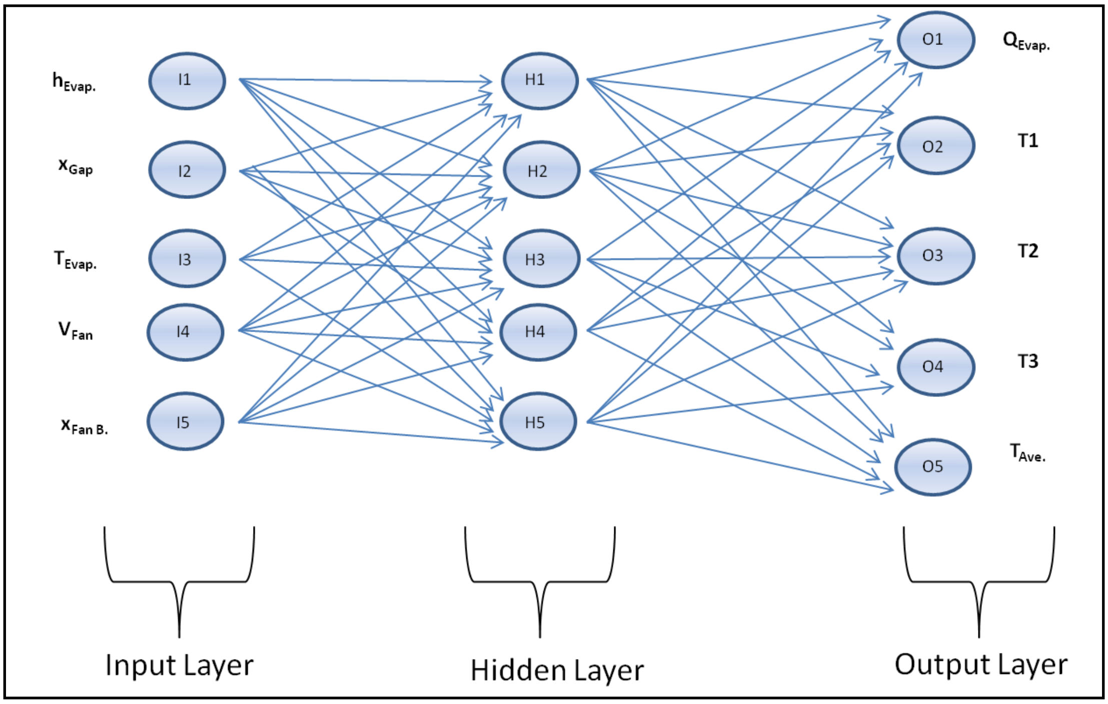

Figure 5.4 The structure of the ANN for the analysis of refrigerator

The performance of an ANN model depends on the characteristics of the network such as the number of hidden layers and the number neurons in each this layer. The network structure was decided to consist of one hidden layer with five neurons along with input and output layer by trial and error with different configurations.

In order to model the ANN for the domestic refrigerator, the calculated data set from the parametric study was divided into training, validating and testing set. The data sets consist of 50 input-output pairs, as listed in Table 5.1. While 90% of the numerical data set was randomly assigned as the training and validation set, the remaining 10% was employed for testing of the network.

Table 5.1 The data sets for modeling ANN

No.	x_{Gap} (mm)	$h_{Evap.}$ (mm)	$x_{Fan\ B.}$ (mm)	$T_{Evap.}$ (C)	V_{Fan} (m/s)	$T_{Ave.}$ (C)	T_1 (C)	T_2 (C)	T_3 (C)	$Q_{Evap.}$ (W)
1	12.00	574.20	346.00	-7.12	2.85	3.51	2.08	1.98	6.49	28.29
2	21.60	868.60	226.70	-5.20	1.75	1.98	2.45	2.38	1.12	30.00
3	11.20	896.20	164.46	-3.60	2.25	3.26	3.03	2.98	3.76	27.41
4	12.40	638.60	325.24	-0.56	1.95	7.42	6.33	6.59	9.35	22.66
5	5.60	565.00	169.65	-2.48	4.15	6.85	3.54	6.51	10.51	23.30
6	18.40	583.40	252.63	-7.44	5.45	2.31	1.55	2.68	2.70	30.74
7	24.00	804.20	283.75	-5.36	4.85	1.68	1.57	1.53	1.94	30.31
8	24.80	611.00	190.39	-4.24	1.85	4.60	4.55	4.67	4.59	27.03
9	6.80	684.60	185.20	-1.84	1.65	6.14	4.78	5.35	8.28	23.48
10	7.20	831.80	159.27	-2.80	4.55	3.60	2.29	2.76	5.74	27.63
11	13.20	482.20	128.15	-5.52	3.75	5.44	3.73	5.20	7.38	25.34
12	7.60	592.60	231.88	-7.76	3.95	2.48	0.19	1.42	5.84	29.41
13	10.80	675.40	148.89	-6.00	5.75	2.39	1.30	2.00	3.88	29.90
14	20.00	905.40	237.07	-1.52	3.65	4.11	4.33	4.03	3.96	26.62
15	9.20	601.80	361.55	-2.32	4.65	5.58	4.08	4.75	7.91	24.09
16	22.80	785.80	335.61	-2.96	2.05	4.23	4.60	3.94	4.16	27.45
17	22.40	629.40	138.52	-5.84	4.95	2.71	2.49	2.26	3.38	29.59
18	14.00	877.80	320.05	-3.28	5.35	2.65	2.42	1.80	3.74	27.35
19	8.80	730.60	117.77	-6.48	3.05	2.72	1.00	1.72	5.46	28.65
20	8.00	850.20	294.12	-1.20	3.25	5.04	4.10	4.47	6.54	24.95
21	18.00	767.40	200.76	-0.72	1.45	6.25	6.01	6.50	6.24	24.37
22	16.80	500.60	268.19	-0.24	4.45	7.98	6.97	8.11	8.85	21.53
23	11.60	822.60	304.49	-3.44	1.15	4.16	4.04	3.50	4.93	26.58
24	8.40	528.20	205.95	-5.68	1.55	5.39	4.49	3.41	8.27	26.55
25	14.40	712.20	122.96	-0.40	3.55	5.87	5.37	5.51	6.72	21.52
26	16.40	555.80	309.68	-4.72	1.05	5.64	4.57	5.33	7.03	25.40
27	19.60	519.00	366.73	-4.40	3.85	5.77	5.04	5.86	6.41	26.10
28	15.20	546.60	154.08	-2.16	5.65	5.73	5.09	5.64	6.47	24.21
29	21.20	795.00	112.59	-3.76	3.45	2.93	3.32	2.44	3.04	27.82
30	12.80	758.20	242.25	-7.60	1.35	1.61	1.24	1.22	2.37	30.30

31	17.60	813.40	174.83	-2.64	5.85	3.33	3.63	2.79	3.57	27.72
32	20.80	776.60	180.01	-7.92	3.35	0.00	0.84	-0.60	-0.24	32.64
33	6.40	841.00	263.00	-6.32	3.15	1.05	0.00	0.78	2.35	30.17
34	23.20	657.00	314.87	-6.96	2.75	2.44	2.16	2.18	3.00	30.54
35	10.00	703.00	247.44	0.00	5.15	6.45	5.38	5.96	8.00	23.72
36	10.40	463.80	278.56	-4.88	5.05	5.23	3.59	4.69	7.42	25.80
37	23.60	473.00	221.51	-3.92	4.25	5.52	5.21	5.37	5.98	25.94
38	24.40	693.80	211.13	-0.88	4.35	5.67	5.58	4.78	6.65	24.42
39	17.20	509.80	143.71	-1.68	2.35	7.78	6.35	8.15	8.84	21.94
40	22.00	537.40	288.93	-1.36	2.15	7.78	6.54	7.80	8.84	22.71
41	15.60	859.40	351.17	-6.16	2.95	1.68	1.61	1.44	2.00	30.85
42	14.80	887.00	195.57	-6.64	4.75	0.00	0.61	-0.61	0.00	31.64
43	9.60	454.60	257.81	-2.00	2.65	7.92	5.50	7.97	10.30	22.68
44	5.20	647.80	330.43	-4.08	2.45	4.33	2.76	3.66	6.58	26.01
45	20.40	620.20	299.31	-3.12	5.95	4.45	4.21	4.49	4.65	27.10
46	19.20	749.00	356.36	-1.04	4.05	5.58	5.45	5.03	6.27	24.55
47	18.80	491.40	216.32	-7.28	2.55	4.06	3.11	4.00	5.05	27.92
48	16.00	666.20	133.33	-5.04	1.25	4.28	3.80	3.96	5.07	26.98
49	13.60	739.80	340.80	-6.80	5.25	1.44	0.67	1.30	2.33	30.27
50	6.00	721.40	273.37	-4.56	5.55	2.92	1.19	1.87	5.69	27.46

Backpropagation algorithm which optimizes the weighted connections by allowing the error to spread from output layer towards the input layers was used as the training systems in training networks. This ANNs algorithm is the most widely used method for engineering applications. Therefore, backpropagation algorithm was selected for training our network.

The prediction of the five output parameters was carried out using a three-layer feed forward backpropagation network. The activation function in the hidden layer was chosen as tangent sigmoid. Linear transfer activation function was used for output layer. Levenberg-Marquardt algorithm was performed for the weighting coefficients in the training procedure.

The output of network was compared to the target output from acquired parametric study at each epoch. The average accuracy of predictions (R) and root-mean-square (rms) values of the outputs error was calculated and defined by (Kreith, 2000, p.631)

$$R = \frac{1}{N} \sum_{i=1}^{N} \frac{A^t}{A^p} \qquad \text{... (5.9)}$$

$$rms = \sqrt{\frac{1}{N}\sum_{i=1}^{N}\left(\frac{A^t - A^p}{A^t}\right)^2} \qquad \text{... (5.10)}$$

where A^p is the predicted results (that is the output of ANN), A^t is the target data (that is parametric results). During the training process of neural network, the performance of the network was evaluated by rms and R.

Finally, the solution of our ANN model was performed with using the package computer code from acquired MATLAB.

CHAPTER SIX
RESULTS AND DISCUSSIONS

6.1 Parametric Study Results

The air flow and temperature distribution inside the domestic refrigerator was investigated numerically and experimentally. Then, parametric study was made to hold a view about the effect of design parameter values change on the performance of the refrigerator. As a result of parametric study, an important criterion is that the interpretation of obtained thousands of data in order to success of the method. It is aim to this parametric study that the optimum design parameter values are defined from these data.

6.1.1 Effects of The Fan Box Location Change

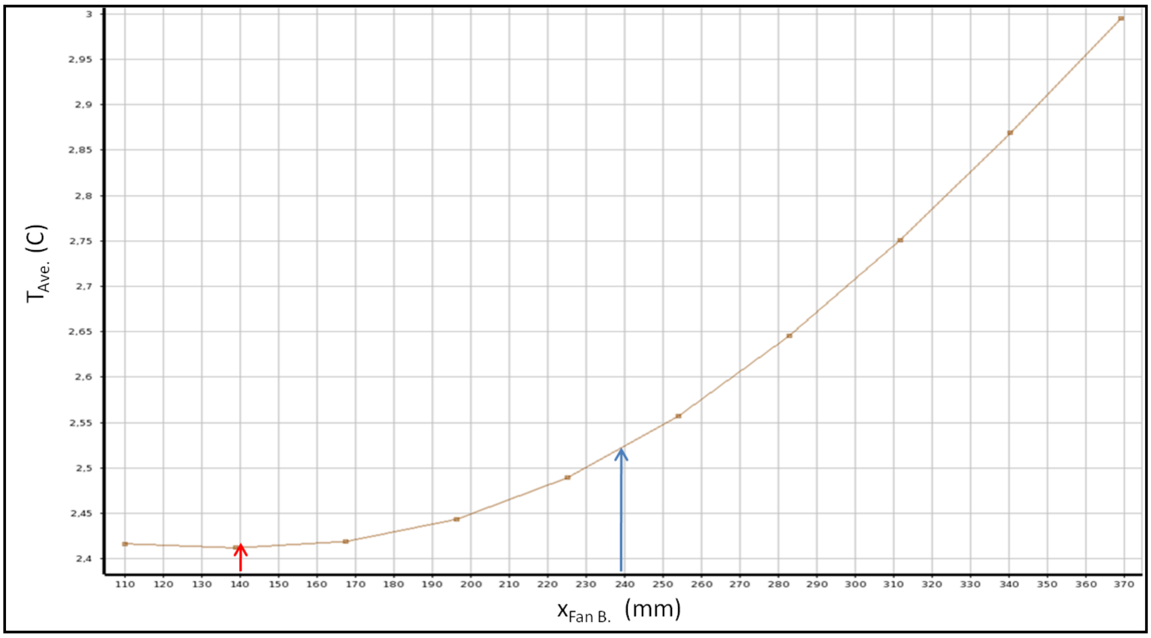

Figure 6.1 The graph of the effects of fan box location change on the average temperature

Figure 6.1 shows us that the effects of fan box location change on the average temperature of thermocouples. As shown in graph, position of the fan box toward the left side wall decreases the average temperature of internal air volume and the positioning toward the right wall increases the average temperature under the current situation. This case occurs due to the operation characteristic of fan and the shape of fan outlets region. So, the horizontal location of fan box doesn't indicate a symmetrical behavior on the average temperature because of the velocity of fan outlet regions different from each other.

When the horizontal placement of fan box is 140 mm on the rear wall, the average temperature can reach the minimum value in case of the value of x_{Gap} 15 mm, h_{Evap} 910 mm, T_{Evap} -3.16 C and V_{Fan} 3.66 m/s.

In Table 6.1, the bold and underlined row is a numerical result for the located fan box at 145 mm in the current situation. While the fan box location is 140 mm in the current situation, 665 mm evaporator height provides the desired conditions. Lower than 665 mm evaporator height doesn't provide the desired temperature of T_{Ave} in the standards.

Table 6.1 In case of the fan box located at 140 mm, determination of the evaporator height for providing the required conditions in the standards

x_{Gap} (mm)	**h_{Evap} (mm)**	**$x_{Fan B.}$ (mm)**	**T_{Evap} (C)**	**V_{Fan} (m/s)**	**T_{Ave} (C)**	**T_1 (C)**	**T_2 (C)**	**T_3 (C)**	**Q_{Evap} (W)**
15	450	140	-3.16	3.66	7.23	5.43	7.20	9.07	23.01
15	550	140	-3.16	3.66	6.21	4.90	6.08	7.67	23.91
15	650	140	-3.16	3.66	5.12	4.30	4.85	6.23	25.18
15	665	140	-3.16	3.66	4.96	4.20	4.66	6.02	25.31
15	750	140	-3.16	3.66	4.04	3.64	3.61	4.89	26.34
15	850	140	-3.16	3.66	3.03	2.96	2.46	3.68	27.34
<u>**15**</u>	<u>**910**</u>	<u>**140**</u>	<u>**-3.16**</u>	<u>**3.66**</u>	<u>**2.41**</u>	<u>**2.49**</u>	<u>**1.84**</u>	<u>**2.91**</u>	<u>**27.82**</u>

6.1.2 Effects of The **Average Velocity of Fan Outlets** *Change*

In the Table 6.2, the relationship between V_{Fan} and h_{Evap} is determined inversely correlated under the same values of x_{Gap}, $x_{Fan\ B.}$, T_{Evap} for providing the desired conditions. By this result, increasing the average velocity of fan outlets reduces the h_{Evap} value. According to the table, it is found that 540 mm evaporator height will be sufficient for the maximum value of V_{Fan} (6 m/s). On the other hand 745 mm evaporator height will require for minimum value of V_{Fan} (1 m/s).

Table 6.2 In case of the fan box located at 140 mm, determination of the evaporator height according to the average velocity of fan outlets change

x_{Gap} (mm)	h_{Evap} (mm)	$x_{Fan\ B.}$ (mm)	T_{Evap} (C)	V_{Fan} (m/s)	T_{Ave} (C)	T_1 (C)	T_2 (C)	T_3 (C)	Q_{Evap} (W)
15	745	140	-3.16	1.00	4.98	4.66	4.84	5.44	24.97
15	720	140	-3.16	2.00	4.97	4.46	4.72	5.75	25.17
15	690	140	-3.16	3.00	4.97	4.29	4.65	5.96	25.28
15	665	140	-3.16	3.66	4.96	4.20	4.66	6.02	25.28
15	650	140	-3.16	4.00	4.97	4.17	4.7	6.04	25.31
15	600	140	-3.16	5.00	4.96	4.09	4.8	6.00	25.32
15	540	140	-3.16	6.00	4.97	4.04	4.95	5.92	25.12

6.1.3 Effects of The Gap Between Evaporator Surface to Glass Shelf Change

In Table 6.3, all combinations provide exceedingly the desired conditions in the standards. The bold and underlined row is a numerical result for the current situation. While the Table 6.3 is examined, increasing the gap distance from 5mm to 15mm decreases the temperature of T_{Ave} and T_3 simultaneously. On the contrary, the gap distance increased from 15 mm to 25 mm raises the temperature of T_{Ave} and decreases the temperature of T_3. The reason is that the decrement quantity of T_3 temperature is less than the total increment quantity of T_1 and T_2 temperature.

According to this table, it is found that T_3 temperature is obtained to be lower than T_1 and T_2 temperatures at first in case of the gap distance at 20 mm.

Table 6.3 Determination of the effect of the gap distance change on the thermocouples' temperature in case of the current situation

x_{Gap} (mm)	h_{Evap} (mm)	$x_{Fan\ B.}$ (mm)	T_{Evap} (C)	V_{Fan} (m/s)	T_{Ave} (C)	T_1 (C)	T_2 (C)	T_3 (C)	Q_{Evap} (W)
5	910	239.67	-3.16	3.66	2.83	1.86	2.04	4.60	27.38
10	910	239.67	-3.16	3.66	2.68	2.26	1.95	3.82	27.53
15	**910**	**239.67**	**-3.16**	**3.66**	**2.52**	**2.51**	**2.06**	**2.99**	**27.90**
20	910	239.67	-3.16	3.66	2.65	3.03	2.37	2.55	28.37
22	910	239.67	-3.16	3.66	2.72	3.19	2.53	2.43	28.55
25	910	239.67	-3.16	3.66	2.85	3.41	2.80	2.35	28.78

It is shown in Table 6.4 that the determination of the required average velocity of fan outlets according to the gap between evaporator surface to glass shelf change for the conditions of $x_{Fan\ B.}$ 140 mm, h_{Evap} 665 mm, and T_{Evap} -3.16 C. The required average velocity of fan outlets will be 2.2 m/s to provide the desired conditions for the maximum values of gap distance (25 mm).

Table 6.4 In case of $x_{Fan\ B.}$ 140 mm, h_{Evap} 665 mm, and T_{Evap} -3.16 C, determination of the average velocity of fan outlets according to the gap between evaporator surface to glass shelf change

x_{Gap} (mm)	h_{Evap} (mm)	$x_{Fan\ B.}$ (mm)	T_{Evap} (C)	V_{Fan} (m/s)	T_{Ave} (C)	T_1 (C)	T_2 (C)	T_3 (C)	Q_{Evap} (W)
5	665	140	-3.16	5.05	4.98	2.82	4.36	7.76	25.12
10	665	140	-3.16	4.30	4.98	3.53	4.51	6.90	25.21
15	665	140	-3.16	3.66	4.96	4.20	4.66	6.02	25.28
20	665	140	-3.16	3	4.96	4.81	4.83	5.26	25.50
25	665	140	-3.16	2.2	4.98	5.32	5.00	4.63	25.83

6.1.4 Effects of The Evaporator Temperature Change

It is taken with Table 6.5 that the determination of the required average velocity of fan outlets according to the evaporator temperature change for the conditions of $x_{Fan\ B.}$ 140 mm, h_{Evap} 665 mm, and x_{Gap} 22 mm. The maximum values of evaporator temperature will be -1.45 C to provide the desired conditions for the maximum values of average velocity of fan outlets (6 m/s). So, higher than this evaporator temperature doesn't provide the desired temperature of T_{Ave} in the standards.

In the Table 6.5, the relationship between V_{Fan} and h_{Evap} is determined directly correlated under the same values of x_{Gap}, $x_{Fan\ B.}$, h_{Evap} in order to providing the desired conditions. By this result, decreasing the evaporator temperature reduces the required V_{Fan} value. Also, the minimum value of the V_{Fan} (1 m/s) provides the desired conditions for the evaporator temperature less than the value of - 4.00 C.

Table 6.5 In case of $x_{Fan\ B.}$ 140 mm, h_{Evap} 665 mm, and x_{Gap} 22 mm, determination of the average velocity of fan outlets according to the evaporator temperature change

x_{Gap} (mm)	h_{Evap} (mm)	$x_{Fan\ B.}$ (mm)	T_{Evap} (C)	V_{Fan} (m/s)	T_{Ave} (C)	T_1 (C)	T_2 (C)	T_3 (C)	Q_{Evap} (W)
22	665	140	0.00	6.00	5.81	5.75	5.82	5.87	24.65
22	665	140	-1.00	6.00	5.23	5.25	5.17	5.29	25.45
22	665	140	-1.45	6.00	4.96	5.00	4.86	5.03	25.84
22	665	140	-2.00	5.10	4.96	5.01	4.84	5.02	25.75
22	665	140	-3.00	3.10	4.96	5.02	4.85	5.02	25.64
22	665	140	-4.00	1.00	4.95	4.99	5.14	4.73	25.61
22	665	140	-5.00	1.00	4.33	4.42	4.58	3.98	26.81

According to Table 6.6, decreasing the evaporator temperature reduces the required evaporator height for the conditions of $x_{Fan\ B.}$ 140 mm, h_{Evap} 665 mm, and

x_{Gap} 22 mm. In addition, when the evaporator temperature is -8 C, the minimum value of evaporator height (450 mm) provides the desired conditions.

Table 6.6 In case of $x_{Fan\ B.}$ 140 mm, V_{Fan} 1 m/s, and x_{Gap} 22 mm, determination of the evaporator height according to the evaporator temperature change

x_{Gap} (mm)	h_{Evap} (mm)	$x_{Fan\ B.}$ (mm)	T_{Evap} (C)	V_{Fan} (m/s)	T_{Ave} (C)	T_1 (C)	T_2 (C)	T_3 (C)	Q_{Evap} (W)
22	605	140	-5.00	1.00	4.97	4.70	5.21	5.01	26.02
22	546	140	-6.00	1.00	4.98	4.45	5.16	5.32	26.53
22	480	140	-7.00	1.00	4.98	4.27	4.98	5.70	26.98
22	450	140	-8.00	1.00	4.57	3.91	4.40	5.41	27.70

6.1.5 Determination of The Optimum Values of Design Parameters

The amount of heat taken from evaporator surface, thermal uniformity of interior air volume and the desired conditions in standards was considered to determine the optimum design parameter values. Thousands of numerical datas are investigated for the optimization of design parameters and then optimum values are determined to be 22 mm gap distance, 665 mm evaporator height, 140 mm fan box location, -2.00 C evaporator surface and 5.5 m/s average velocity of fan outlets. In the Table 6.7, the bold and underlined row is a numerical result for the optimum case. So, the amount of heat taken from evaporator surface will be improved approximately 2 Watt. As a result, the annual energy consumption will be decreased 17.52 kW.

Table 6.7 The optimum design parameter values

x_{Gap} (mm)	h_{Evap} (mm)	$x_{Fan\ B.}$ (mm)	T_{Evap} (C)	V_{Fan} (m/s)	T_{Ave} (C)	T_1 (C)	T_2 (C)	T_3 (C)	Q_{Evap} (W)
<u>22</u>	**<u>665</u>**	**<u>140</u>**	**<u>-2.00</u>**	**<u>5.5</u>**	**<u>4.80</u>**	**<u>4.66</u>**	**<u>4.86</u>**	**<u>4.67</u>**	**<u>26.00</u>**
15	910	239,67	-3.16	3.66	2.52	2.51	2.06	2.99	27.90

6.2 ANNs Study Results

Artificial neural networks are widely accepted as a method offering an alternative way to solve complex and ill-defined problems. They can perform prediction and generalization at high speed. Thereby, the design parameters of domestic refrigerator which are independent of each other were investigated on the effect of intended conditions inside the domestic refrigerator and were optimized at short time by using ANNs method. It is aim to use this method that feasible design parameter values can be predicted previously in the design and optimization process of domestic refrigerators, rapidly

The numerical data sets consist of 50 input-output pairs While 45 of the numerical data set was randomly assigned as the training and validation set, the remaining 5 was employed for testing of the network.

A scatter plot of the modeled ANN performance, end of the training and validation process, is shown in Figure 6.2. The black straight line indicates perfect prediction and it is used to evaluate the accuracy of the ANN prediction. Other red and purple lines show ±10% error band. Almost all ANN output values shown with the blue dots are within this error band. The ANN model can estimate for determined output parameters in root-mean-square (rms) of 0.01, the accuracy of prediction (R) of 0.994 and mean relative error (MRE) of 6.68% with the results of parametric study.

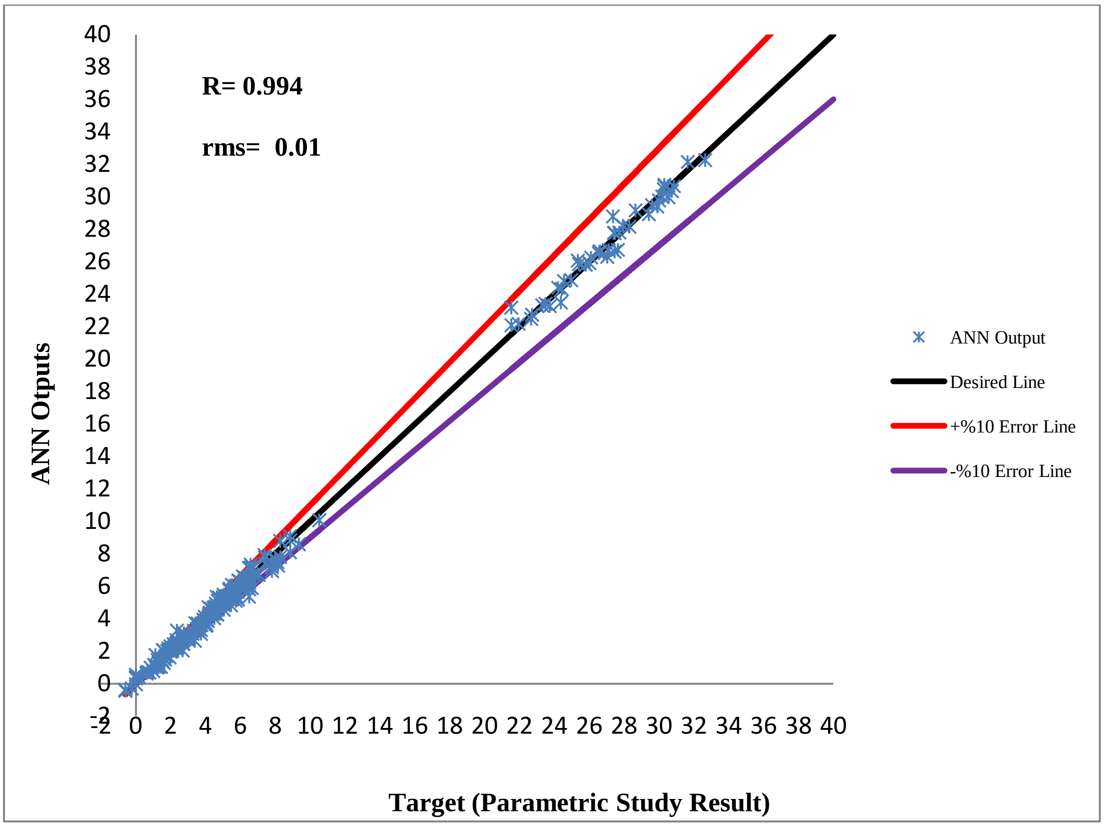

Figure 6.2 The scatter plot of the network performance, end of the training and validating process

After the training and validation process, five set of test data acquired from parametric result with calculating numerical analysis were given to the ANN model for testing network performance, which was not introduced to the network during training. Input parameter values of test data which were selected randomly are shown in Table 6.8. Then ANN model could predict output values in seconds for these sets data. If numerical analysis were used to calculate these output values, it would have taken at least fifteen hours.

Table 6.8 Input parameters and values of test data

	x_{Gap} (mm)	h_{Evap} (mm)	$x_{Fan\ B.}$ (mm)	T_{Evap} (C)	V_{Fan} (m/s)
Set 1	9.20	601.80	361.55	-2.32	4.65
Set 2	21.20	795.00	112.59	-3.76	3.45
Set 3	23.60	473.00	221.51	-3.92	4.25
Set 4	9.60	454.60	257.81	-2.00	2.65
Set 5	16.00	666.20	133.33	-5.04	1.25

Table 6.9 shows that comparison of ANN prediction and parametric result evaluated numerically for the average temperature of thermocouples (T_{Ave}). For the T_{Ave}, the maximum absolute difference is 0.17 C and the maximum relative error is less than 3.10 %. It can be observed that the relative error values are in the range of 0.15 – 3.06 %.

Table 6.9 Comparison of the parametric result evaluated numerically and using the ANNs model for T_{Ave}

T_{Ave} (C)	Parametric Result (C)	ANN Prediction (C)	Absolute Difference (C)	Relative Error (%)
Set 1	5.58	5.75	0.17	3.06
Set 2	2.93	2.89	0.04	1.31
Set 3	5.52	5.39	0.13	2.41
Set 4	7.92	7.91	0.01	0.15
Set 5	4.28	4.32	0.04	1.05

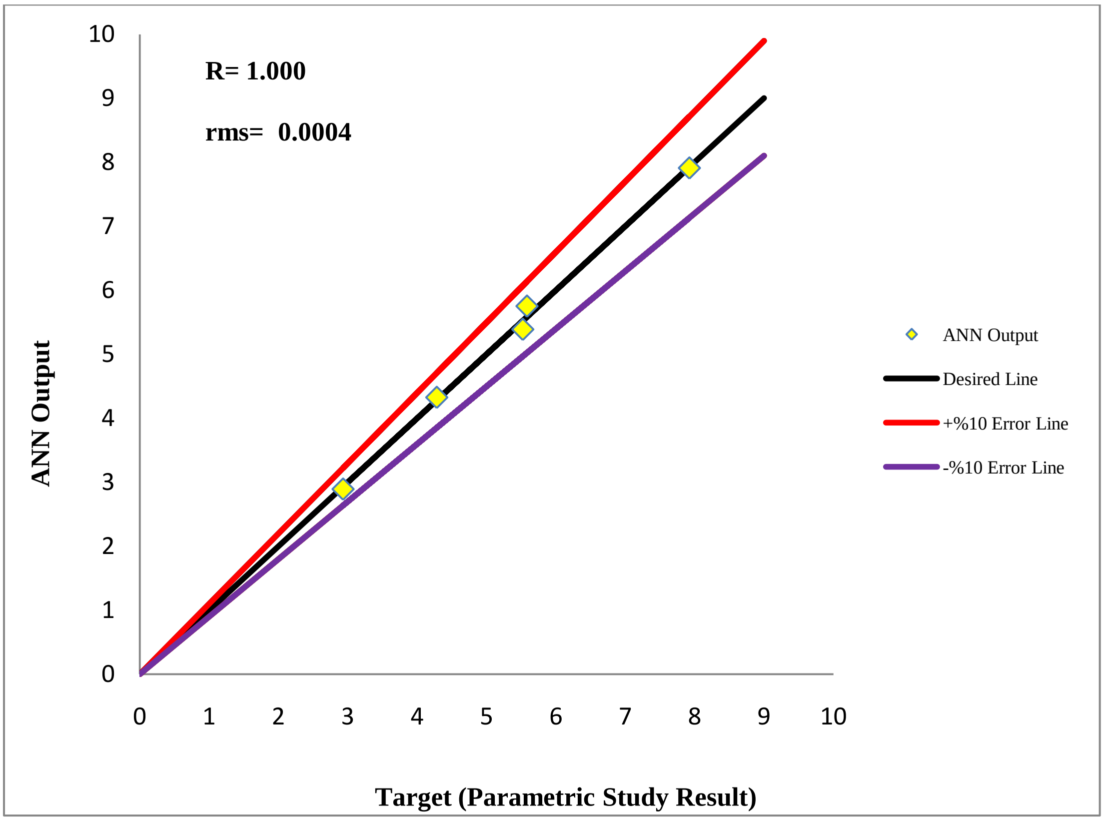

Figure 6.3 Comparison between target and ANN output as scatter plot for T_{Ave}

A scatter plot of comparison between target and ANN output for T_{Ave}, is shown in Figure 6.3. All ANN output values shown with the yellow dots are within this error band and so closed to desired line. The ANN model can estimate for T_{Ave} in the root-mean-square (rms) of 0.0004, the accuracy of prediction (R) of 1.000, the mean relative error (MRE) of 1.59% and mean absolute error of 0.08 C.

Table 6.10 shows that comparison of ANN prediction and parametric result evaluated numerically for the temperature of T_1. For the T_1, the maximum absolute difference is 0.40 C and the maximum relative error is less than 8.70 %. It can be observed that the relative error values are in the range of 1.01 – 8.64 %.

A scatter plot of comparison between target and ANN output for T_1, is shown in Figure 6.4. All ANN output values shown with the yellow dots are within this error band and so closed to desired line. The ANN model can estimate for T_1 in the root-mean-square (rms) of 0.003, the accuracy of prediction (R) of 1.021, the mean relative error (MRE) of 4.82% and mean absolute error of 0.22 C.

Table 6.10 Comparison of the parametric result evaluated numerically and using the ANNs model for T_1

T_1 (C)	**Parametric Result (C)**	**ANN Prediction (C)**	**Absolute Difference (C)**	**Relative Error (%)**
Set 1	4.08	4.12	0.04	1.01
Set 2	3.32	3.36	0.04	1.23
Set 3	5.21	4.81	0.40	7.76
Set 4	5.50	5.80	0.30	5.45
Set 5	3.80	3.47	0.33	8.64

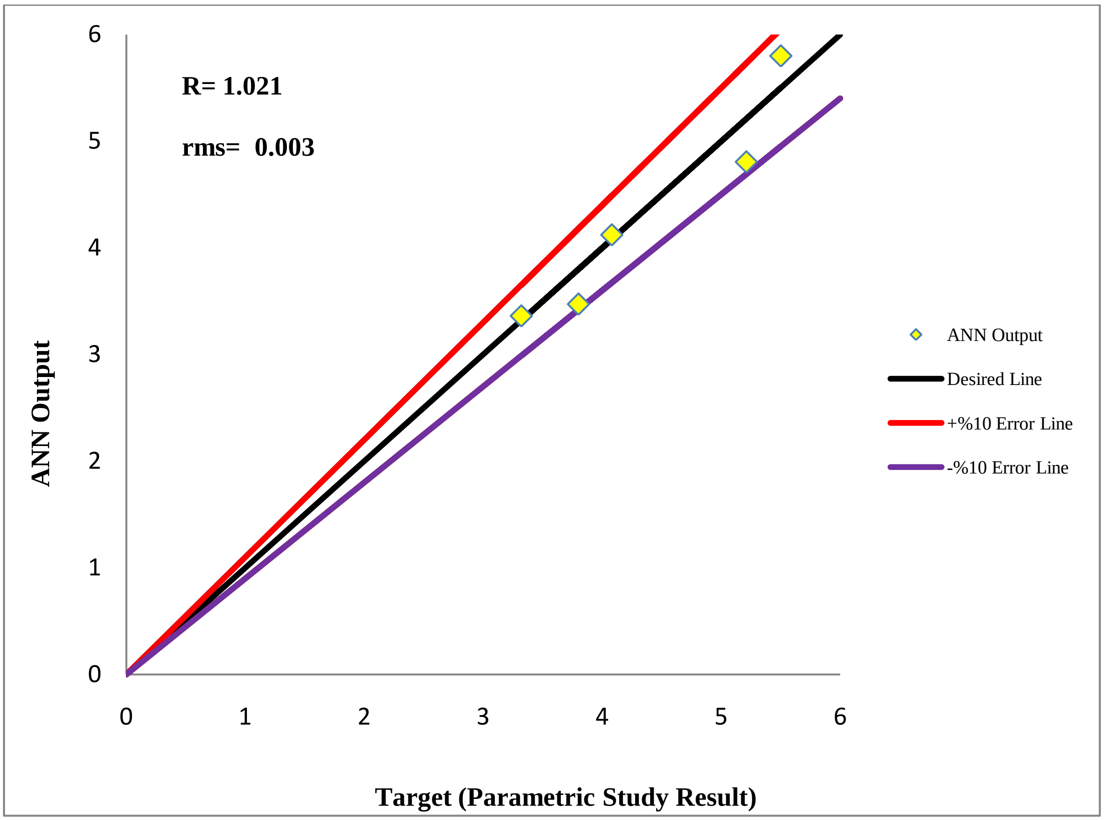

Figure 6.4 Comparison between target and ANN output as scatter plot for T_1

Table 6.11 shows that comparison of ANN prediction and parametric result evaluated numerically for the temperature of T_2. For the T_2, the maximum absolute difference is 0.54 C and the maximum relative error is less than 11.50 %. It can be observed that the relative error values are in the range of 0.39 – 11.43 %.

Table 6.11 Comparison of the parametric result evaluated numerically and using the ANNs model for T_2

T_2 (C)	**Parametric Result (C)**	**ANN Prediction (C)**	**Absolute Difference (C)**	**Relative Error (%)**
Set 1	4.75	5.29	0.54	11.43
Set 2	2.44	2.57	0.13	5.46
Set 3	5.37	5.16	0.21	3.90
Set 4	7.97	7.57	0.40	5.04
Set 5	3.96	3.98	0.02	0.39

A scatter plot of comparison between target and ANN output for T_2, is shown in Figure 6.5. Almost ANN output values shown with the yellow dots are within this error band and so closed to desired line. The ANN model can estimate for T_2 in the root-mean-square (rms) of 0.004, the accuracy of prediction (R) of 0.987, the mean relative error (MRE) of 5.24% and mean absolute error of 0.26 C.

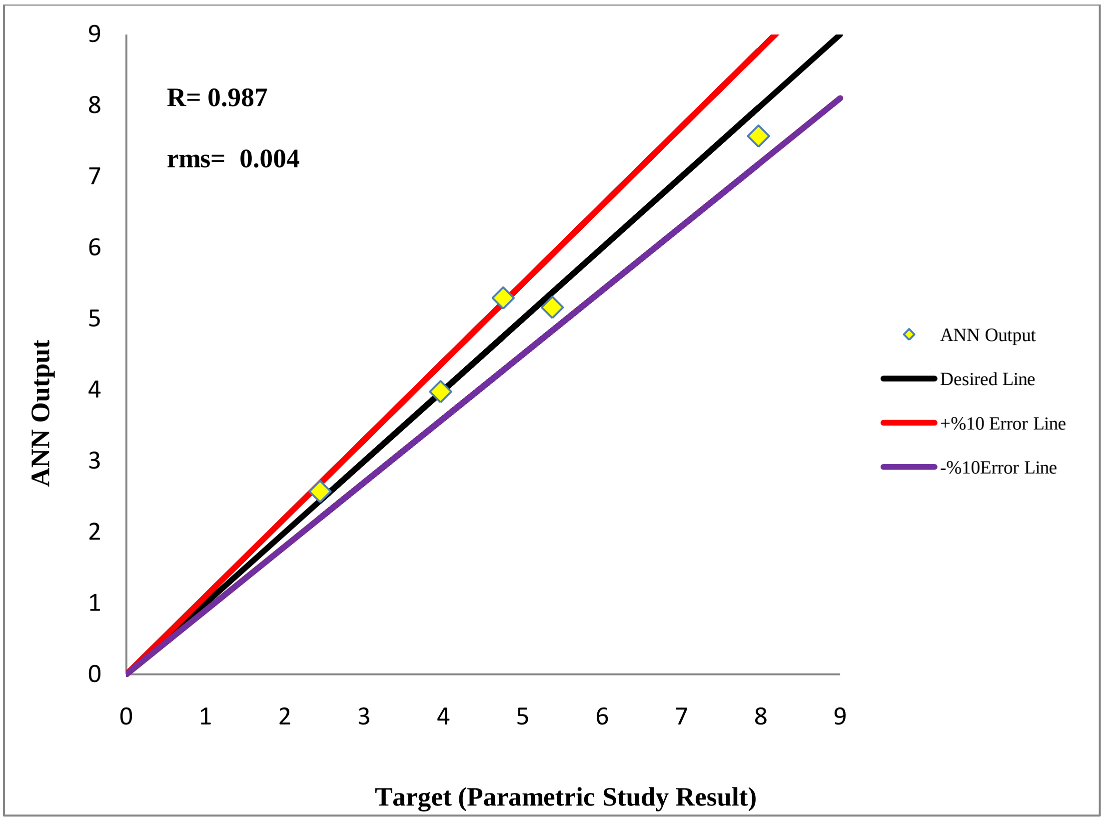

Figure 6.5 Comparison between target and ANN output as scatter plot for T_2

Table 6.12 shows that comparison of ANN prediction and parametric result evaluated numerically for the temperature of T_3. For the T_3, the maximum absolute difference is 0.47 C and the maximum relative error is less than 10.30 %. It can be observed that the relative error values are in the range of 0.77 – 10.22 %.

A scatter plot of comparison between target and ANN output for T_3, is shown in Figure 6.6. Almost ANN output values shown with the yellow dots are within this error band and so closed to desired line. The ANN model can estimate for T_3 in the root-mean-square (rms) of 0.004, the accuracy of prediction (R) of 0.999, the mean relative error (MRE) of 4.93% and mean absolute error of 0.23 C.

Table 6.12 Comparison of the parametric result evaluated numerically and using the ANNs model for T_3

T_3 (C)	**Parametric Result (C)**	**ANN Prediction (C)**	**Absolute Difference (C)**	**Relative Error (%)**
Set 1	7.91	7.84	0.07	0.83
Set 2	3.04	2.73	0.31	10.22
Set 3	5.98	6.20	0.22	3.60
Set 4	10.30	10.38	0.08	0.77
Set 5	5.07	5.54	0.47	9.20

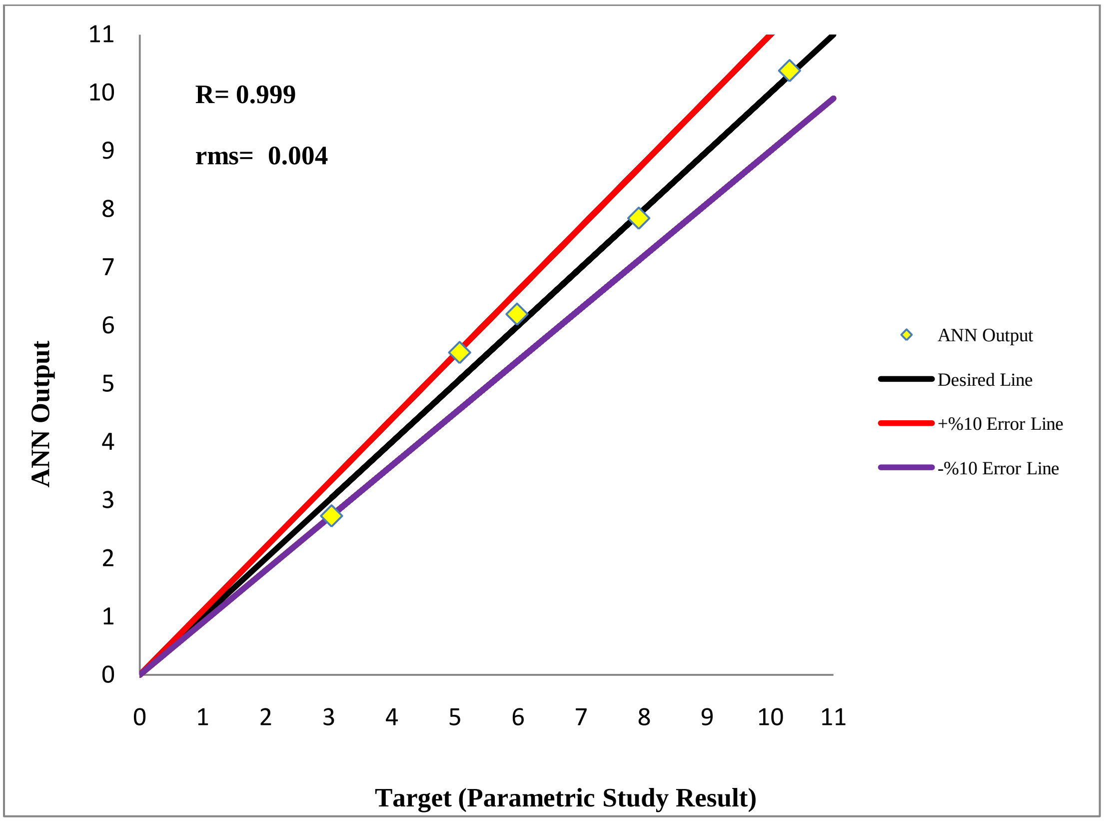

Figure 6.6 Comparison between target and ANN output as scatter plot for T_3

Table 6.13 shows that comparison of ANN prediction and parametric result evaluated numerically for the amount of heat taken from evaporator surface (Q_{Evap}). For the Q_{Evap}, the maximum absolute difference is 0.54 W and the maximum relative error is less than 2.30 %. It can be observed that the relative error values are in the range of 0.45 – 2.24 %.

A scatter plot of comparison between target and ANN output for Q_{Evap}, is shown in Figure 6.7. All ANN output values shown with the yellow dots are within this error band and so closed to desired line. The ANN model can estimate for Q_{Evap} in the root-mean-square (rms) of 0.0002, the accuracy of prediction (R) of 1.00, the mean relative error (MRE) of 2.24% and mean absolute error of 0.28 W.

Table 6.13 Comparison of the parametric result evaluated numerically and using the ANNs model for Q_{Evap}

Q_{Evap} (W)	Parametric Result (W)	ANN Prediction (W)	Absolute Difference (W)	Relative Error (%)
Set 1	24.09	24.63	0.54	2.24
Set 2	27.82	27.99	0.17	0.62
Set 3	25.94	25.63	0.31	1.19
Set 4	22.68	22.41	0.27	1.18
Set 5	26.98	26.86	0.12	0.45

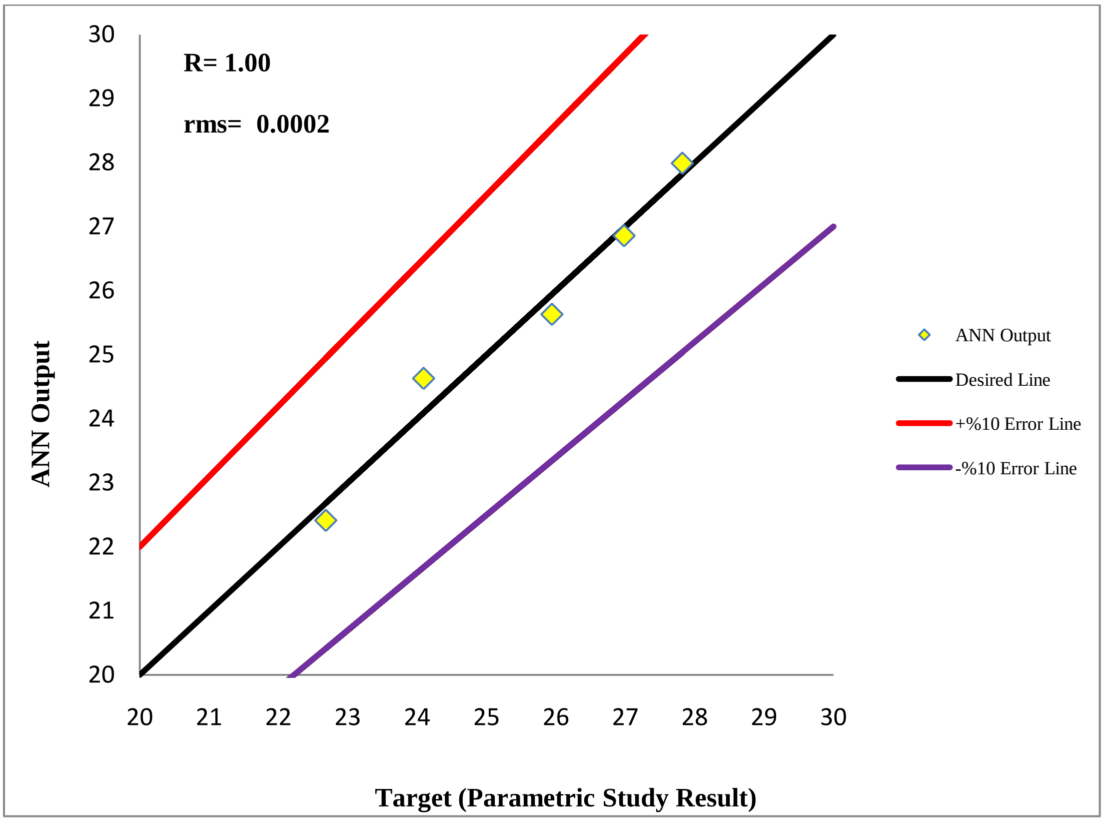

Figure 6.7 Comparison between target and ANN output as scatter plot for Q_{Evap}

After the testing process, the output values of the optimum design case determined parametrically is predicted by our ANNs model. Table 6.14 shows that comparison of ANN prediction and parametric result evaluated numerically for the optimum design case. For the output values of best design, the mean relative error is 2.11 % and the maximum relative error is less than 5.20 %. It can be observed that the relative error values are in the range of 0.8 – 5.14 %.

Table 6.14 Comparison of the parametric result evaluated numerically and using the ANNs model for best design

Optimum Design Case	**Parametric Result**	**ANN Prediction**	**Absolute Difference**	**Relative Error (%)**
$\mathbf{T_{Ave}}$	4.80 C	4.72 C	0.08 C	1.67
$\mathbf{T_1}$	4.86 C	4.79 C	0.07 C	1.44
$\mathbf{T_2}$	4.67 C	4.43 C	0.24 C	5.14
$\mathbf{T_3}$	4.88 C	4.92 C	0.04 C	0.82
$\mathbf{Q_{Evap}}$	26.00 W	25.62 W	0.38 W	1.46

Finally, the ANNs results reveal that domestic refrigerator can alternatively be modeled using ANNs rather than the hardest one to model using classical techniques such as trial and error method in order to optimize its design parameters.

CHAPTER SEVEN
CONCLUSIONS

The aim of this thesis is to optimize the design parameters of domestic refrigerator with using parametric and ANNs methods according to the temperature and air flow distributions of internal air volume. In the literature researchers, numerical and experimental techniques for various type refrigerators and ANNs method for components performance of refrigeration system were examined. These researchers showed that none of these studies involves numerical, parametric and ANNs methods together for determining optimum design parameter's values of domestic refrigerators. To resolve this deficiency, an optimization method was developed.

At the beginning of this study, domestic refrigeration systems and their standards were investigated. Numerical solution methodologies and optimization technique were examined and also an experimental study was made in order to verify our numerical model.

For numerical study, three dimensional model of interior air volume of the static type refrigerator was prepared and Computational Fluid Dynamics and Heat Transfer (CFDHT) analyses were made. The heat and flow transfer of internal air is analyzed with almost real model of the refrigerator interior cabinet. Verification of the numerical study was performed with the measurements which were made from the TGET department's test room of Vestel White Goods Company. It is observed that numerical and experimental results were all in coherence within acceptable limits. The average absolute difference of thermocouple temperatures between actual model and numerical model is 0.84 C

In order to show the applicability of the ANN modeling to domestic refrigerators, a network structure based on backpropagation algorithm has been developed to predict various output parameters of a single door static type domestic refrigerator. A parametric study was made by using the parametric design section of a commercial analysis program in order to investigate the effects of the determined inner design parameters on the refrigerator's performance and acquire data sets for training and testing our ANN model. The ANN modeling for domestic refrigerator demonstrates to us a good statistical performance with the average accuracy of predictions of 0.999 and average relative mean errors of 3.54%.

The utility of this study is developing an optimization method for domestic refrigerators' design parameters using the numerical methods and the ANNs techniques together for the performance and the design process improvement studies in a faster and cheaper way. In conclusion, our study is shown that this optimization method can be used as a tool by the designers and engineers in the process of research and development

This thesis is taking placement under 00457.STZ.2009-2 encoded SANTEZ project study and scope of this thesis is to provide and develop an optimization method for design parameters of domestic refrigerators.

REFERENCES

Afonso, C., & Matos, J. (2006). The effect of radiation shields around the air condenser and compressor of a refrigerator on the temperature distribution inside it. *International Journal of Refrigeration* (29), 1144-1151.

Amara, S. B., Laguerre, O., Mojtabi, M. C. C., Lartigue, B., & Flick, D. (2008). Piv measurement of the flow field in a domestic refrigerator model: Comprasion with 3d simulations. *International Journal of Refrigeration* (31), 1328-1340.

Antonio, C. C., & Afonso, C. F. (2011). Air temperature fields inside refrigeration cabins: A comprasion of results from cfd and ann modeling. *Applied Thermal Engineering* (31), 1244-1251.

ASHRAE (American Society of Heating, Refrigerating and Air-Conditioning Engineers) (2006), *Refrigeration handbook*.

Ayata, T., Çavuşoğlu, A., & Arcaklıoğlu, E. (2006). Predictions of temperature distributions on layered metal plates using artificial neural networks. *Energy Conversion and Management* (47), 2361-2370.

Cengel, Y. A., & Boles, M. A. (2006). *Thermodynamics an engineering approach* (5th ed.). McGraw Hill.

Cortella, G., Manzan, M., & Comini, G. (2001). CFD simulation of refrigerated display cabinets. *International Journal of Refrigeration* (24), 250-260.

D'Agaro, P., Cortella, G., & Croce, G. (2006). Two- and three-dimensional cfd applied to vertical display cabinets simulation. *International Journal of Refrigeration* (29), 178-190.

Dinçer, İ., & Kanoğlu, M. (2010).*Refrigeration systems and application* (2th ed.). Chichester: Wiley.

Ding, G. L., Qiao, H. T., & Lu, Z. L. (2004). Ways to improve thermal uniformity inside a refrigerator. *Applied Thermal Engineering* (24), 1827-1840.

Ertunc, H. M., & Hosoz, M. (2006). Artificial neural networks analysis of a refrigeration system with an evaporative condenser. *Applied Thermal Engineering* (26), 627-635.

Foster, A. M., Madge, M., & Evans, J. A. (2005). The use of cfd to improve the performance of a chilled multi-deck retail display cabinet. *International Journal of Refrigeration* (28), 698-705.

Fukuyo, K., Tanaami, T., & Ashida, H. (2003). Thermal uniformity and rapid cooling inside refrigerators. *International Journal of Refrigeration* (26), 249-255.

Gupta, J. K., Gopal, M. R., & Chakraborty, S. (2007). Modeling of a domestic frost-free refrigerator. *International Journal of Refrigeration* (30), 311-322.

Haykin, S. (1999). *Neural networks a comprehensive foundation* (2th ed.). Delhi: Prentice Hall.

Incropera, F. P., DeWitt, D. P., Bergman, T. L., & Lavine, A. S. (2006). *Fundamentals of heat and mass transfer (6th ed.).* Chichester: Wiley.

Islamoglu, Y. (2003). A new approach for the prediction of the heat transfer rate of the wire-on-tube type heat exchanger-use of an artificial neural network model. *Applied Thermal Engineering* (23), 243-249.

ISO 15502 (International Organization for Standardization 15502) (2005). *Household refrigerating appliance-characteristic and test methods*.

Kalogirou, S. A. (2000). Applications of artificial neural-networks for energy systems. *Applied Energy* (67), 17-35.

Khemani, H. (January, 2010). *Types of refrigeration evaporators*. Retrieved December, 2010, from http://www.brighthub.com/engineering/mechanical/articles/61270.aspx.

Khemani, H. (January, 2010). *Types of refrigeration evaporators*. Retrieved December, 2010, from http://www.brighthub.com/engineering/mechanical/articles/61270.aspx ?p=2.

Khemani, H. (December, 2010). *Capillary tube for refrigeration and air conditioning systems.* Retrieved December, 2010, from http://www.brighthub.com/engineering/mechanical/articles/58420.aspx.

Kreith, K. (2000). *The crc handbook of thermal engineering.* Boca Raton: Crc Press.

Laguerre, O., & Flick, D. (2004). Heat transfer by natural convection in domestic refrigerators. *Journal of Food Engineering* (62), 79-88.

Laguerre, O., Amara, S. B., Moureh, J., & Flick, D. (2007). Numerical simulation of air flow and heat transfer in domestic refrigerators. *Journal of Food Engineering* (81), 144-156.

MATLAB (Mathematic Laboratuary) *Neural toolbox 6 user's guide.* (2008)

Orlando, D., Rodriguez, N., & Consalter, L. A. (2009). Neural network for cost estimation of shell and tube heat exchangers. *Expert Systems with Applications* (36), 7435-7440.

Peng, H., & Ling, X. (2008). Optimal design approach for the plate-fin heat exchangers using neural networks cooperated with genetic algorithms. *Applied Thermal Engineering* (28), 642-650.

Ramgopal, M. (2006). *Condenser and evaporator.* Retrieved December, 2010, from http://nptel.iitm.ac.in/courses/Webcourse-contents/IIT Kharagpur/Ref and Air Cond/pdf/R&AC Lecture 22.pdf.

Saedodin, S., Torabi, M., Naserian, R. S., & Salehi, P. (2010). A combined experimental and three-dimensional numerical study of natural convection heat transfer in a domestic freezer for optimization and temperature prediction. *International Review of Mechanical Engineering* (4), n.6.

Swider, D. J., Browne, M. W., Bansal, P. K., & Kecman, V. (2001). Modelling of vapour-compression liquid chillers with neural networks. *Applied Thermal Engineering* (21), 311-329.

Vega, A. P., Sen, M., Yang, K. T., & McClain, R. L. (2001). Neural network analysis of fin-tube refrigerating heat exchanger with limited experimental data. *International Journal of Heat and Mass Transfer* (44), 760-770.

Wikipedia (n.d.) Retrieved December, 2010, from http://en.wikipedia.org/wiki/Refrigerator.

Xie, G. N., Wang, Q. W., Zeng, M., & Luo, L. Q. (2007). Heat transfer analysis for shell-and-tube heat exchangers with experimental data by artificial neural networks approach. *Applied Thermal Engineering* (27), 1096-1104.

Xie, G., Sunden, B., Wang, Q., & Tang, L. (2009). Performance peridictions of laminar and turbulent heat transfer and fluid flow of heat exchangers having large tube-diameter and large tube-row by artificial neural networks. *International Journal of Heat and Mass Transfer* (52), 2484-2497.

Yilmaz, S., & Atik, K. (2007). Modeling of a mechanical cooling systems with variable cooling capacity by using artificial neural network. *Applied Thermal Engineering* (27), 2308-2313.

Zhao, L. X., & Zhang, C. L. (2010). Fin-and-tube condenser performance evaluation using neural networks. *International Journal of Refrigeration* (33), 625-634.